HEAT CONDUCTION IN LOW DIMENSIONAL LATTICE SYSTEMS

by

VENKATESHAN KANNAN

A dissertation submitted to the
Graduate School-New Brunswick
Rutgers, The State University of New Jersey
in partial fulfillment of the requirements
for the degree of
Doctor of Philosophy
Graduate Program in Physics and Astronomy
Written under the direction of
Prof. Joel Lebowitz
and approved by

_____

_____

_____

_____

_____

New Brunswick, New Jersey

JANUARY 2013

ABSTRACT OF THE DISSERTATION

HEAT CONDUCTION IN LOW DIMENSIONAL LATTICE SYSTEMS

By VENKATESHAN KANNAN

Dissertation Director:

Prof. Joel Lebowitz

We study heat conduction and other nonequilibrium properties of one dimensional chain of particles, ordered and disordered, harmonic and anharmonic. Our results include derivation of oscillatory temperature profile for harmonic alternating mass chains, demonstration of finite heat conductivity for disordered harmonic chains with velocity-flipping noise, description of fluctuations for ordered harmonic systems with noise, and understanding the behavior of systems with noise and anharmonicity. We provide a comparative analysis of the effects of the various dynamics and system parameters on the characteristics of the nonequilibrium steady state of the chain.

Acknowledgements

I am stating the obvious in noting that the progress during a doctoral program depends on various factors. A crucial aspect that has great professional and personal significance is all the people who support and encourage your efforts, in some cases directly and obviously, but in several others, make contributions in rather subtle and unseen ways.

I have been very fortunate that the people connected to my work have all had a very positive effect on my research and learning. To begin with, I cannot thank my advsior, Prof. Joel Lebowitz enough. It is hard for me to think of any way in which I could have had a better supervisor. His guidance exemplified the perfect balance between directing the research at important points and providing sufficient space and freedom for me to be able to explore the subject on my own. His advice is always very sharp and his vast experience enables him to immediately recognize the underlying source of any problem I may bring to his attention. Although very busy with his schedule, he has always been willing to meet me whenever I needed help, even during trips overseas when we would be in touch over email. Needless to mention, his insights on the problem of heat conduction and statistical mechanics in general, had a considerable influence in shaping my view of the subject.

I am very grateful to Prof. Abhishek Dhar, who has been a mentor and collaborator

on a number of topics over the course of my Phd. It does not happen often that a graduate student is surrounded by researchers who are all on top of their field but that was my case. Prof. Dhar had an advanced and a very thorough understanding of the subject of transport phenomena and I learned a lot in the discussions I've had with him. Doubts and questions that arise on reading the literature are often explained away in such short but focused conversations.

I've been very fortunate to have had comparable conversations with Prof. Jani Lukkarinen and Prof. Cedric Bernardin as well. Their visits to the Rutgers campus would invariably include blackboard sessions where various theoretical ideas, numerical approaches and unresolved problems are proposed and explained. These have been an integral part of my graduate training.

It is impossible to overstate the important role of my parents, L.Kannan and K.Kamala, during this period. My knowledge of their unconditional support for me has been the pivotal source of my stability and provided the courage to pursue my aims. I owe it to them for their many sacrifices for my education, now and earlier as well.

There have been other friends and family who have been supportive and encouraging. A Phd. can be a stressful time and it is necessary to cultivate other interests and passions to keep your spirit up. There have been a revolving set of people who've helped me do with that and I thank all of them for it. I've met some in unusual circumstances but that has only made it all the more exciting.

Finally, I would like to thank the Physics department at Rutgers University. I was never burdened with rules or conditions or impositions against freedom other than the most minimal and reasonable requirements. The graduate directors during my

period, Prof. Ransom and Prof. Williamns, have always been very approachable and swiftly resolve whatever issue I may have had. The graduate secretary, Ms. Hinds, has been helpful too. I would like to use this opportunity to thank the two secretaries in the math department, Leszita Townsend and Hope diCapua, for all the assistance I've received from them.

Contents

List of Figures

List of Tables

Chapter 1

Introduction

Heat conduction is a very common phenomena, witnessed both in everyday experiences and in standard engineering applications, and it is normally assumed that we understand the process very well. To a certain extent, this view is correct. As it happens, heat conduction in almost all known materials is empirically found to obey Fourier's Law, according to which the heat current is proportional to (negative of) the temperature gradient. In three dimensions, we have :

$$J = -\kappa \nabla T \tag{1.1}$$

where J is the current per unit area and the constant of proportionality κ is the heat conductivity, a property of the material that depends on the temperature, pressure, etc. This macroscopic equation is empirically found to be valid for a wide class of materials, and this relation is taken to be the correct description of heat transport in most engineering analysis. And yet, despite the seeming universality of this relation, there is no rigorous derivation of this equation starting from the microscopic dynamics, either classical or quantum. It is this unresolved problem of heat conduction that we wish to investigate in our work.

We shall limit our study here to the classical case as (1.1) is also seen to be valid in molecular dynamical simulations of Newton's equations, as will be discussed later. More concretely, we consider a lattice governed internally by Hamiltonian dynamics, of length l, with fixed cross section area, and ends connected to thermal reservoirs that are maintained at fixed unequal temperatures T_a and T_b. Given the Hamiltonian dynamics and also the interactions of the ends with reservoirs, the challenge is to prove that the heat flow at steady state would be given by

$$J \propto \frac{T_a - T_b}{l} \tag{1.2}$$

There have been a multitude of attempts to derive this equation for various systems over a span of more than half a century. While there has not yet been an all-encompassing rigorous derivation of this relation for a system with realistic dynamics, a vast literature has emerged in the last few decades revealing several intriguing aspects of the problem. In addition to many ingenious models that have been proposed and successfully solved, a large number of insightful ideas and mathematical results have sprung up from the study of these systems.

1.1 Overview Of Important Results

One of the earliest results in the study of heat conduction was the rigorous demonstration that uniform (also described as *ordered*) or periodic lattices with harmonic interactions have a heat current J that is independent of the number of particles N along the direction of flow, i.e, the conductivity κ_N, defined as $\frac{J_N}{(T_a - T_b)/N}$, grows as N[2, 20]. This behavior can be physically explained by the ballistic transport of phonons inside the crystal (see Chapter 2 for more discussion).

Instead of the ordered system, if we had the particle masses to be random, e.g., each mass was chosen from a fixed i.i.d, it produces the localization of vibrational modes of the lattice. The extent to which a particular mode is localized depends on the frequency of that mode and the dimension of the lattice. In such *disordered* lattices, it is only the delocalized modes (if there are any) that carry the current. In one-dimension, where the system is studied quite thoroughly, it has been shown that, for lattices with on-site pinning (also called *pinned lattice*) in the bulk, where there is a gap in the vibrational spectrum, the conductivity decays exponentially with the size of the system, regardless of the boundary conditions [34]. Such models with pinning in the bulk physically corresponds to attaching the lattice to a substrate. For the disordered system that is unpinned in the bulk, the heat current depends on the nature of the boundary conditions and the spectral properties of the heat baths [22].

The dynamics of real physical materials include complicated interactions that goes beyond the harmonic nearest neighbor dynamics considered above. An indirect way to model the effects of these non-harmonic interactions is by introducing stochastic dynamics within the bulk. An excellent example that is not very physical but illustrative of the significance of stochastic noise is the KMP model [5], where a one dimensional chain of oscillators interact only by the random redistribution of energy between neighboring particles. This particular model was solved exactly and the heat current obeys Fourier's Law.

A large number of interesting results have been obtained for other systems with random dynamics. It has been proven for ordered lattices with stochastic noise that conserve both momentum and energy, that regular conductivity in obtained in dimension $d \geq 3$ and superdiffusive heat transport holds for lower dimensions [25]. When the same dynamic appears in a pinned lattice, or one with a momentum non-

conserving noise, regular transport is obtained in all dimensions $d \geq 1$ [26].

A system with a very different type of stochastic interaction is a lattice with self-consistent reservoirs. In this model, every site in the lattice interacts with a thermal reservoir, whose temperature is determined by the self-consistency condition at steady state which requires that there is no net energy exchange between the intermediate particle and its reservoir [27]. It was proved that Fourier's Law is satisfied for this system in any dimension [29].

What happens when stochastic noise is introduced in a disordered lattice? This problem has been studied only recently, and it has been shown for an energy conserving noise in general d dimensional lattice, that we get a finite conductivity[32].

While the stochastic dynamics acts as a substitute for the complex interactions found in physical systems, in order to accurately model a realistic system, it is necessary to incorporate the nonlinear interaction between sites of the lattice. However, analyzing systems with anharmonic interactions is notoriously difficult and most results for such systems have been obtained using numerical computations and molecular dynamical simulations.

There is growing numerical evidence that the conductivity is finite for one dimensional pinned chains with anharmonic interactions[12, 45, 47, 11]. Analytic approaches in investigating lattices with quartic pinning potential using kinetic theory of phonons (Peierls-Boltzmann equation) have also pointed to existence of finite conductivity[13, 14].

For unpinned one-dimensional ordered systems with anharmonic interaction, such as

the FPU β chain (nearest neighbor potential has both harmonic and quartic components), numerical simulations indicate that $\kappa \sim N^{\alpha}$ where the $1/3 \leq \alpha < 1/2$ [7, 8, 9]. Applying the phonon kinetic theory to the system suggests that $\alpha = 0.4$[10].

In two-dimensional homogeneous unpinned lattices with anharmonic interaction, molecular dynamical simulations for both FPU-β type interaction and Lennard-Jones potential ($V(q) = \epsilon[(\frac{\sigma}{q})^{12} - (\frac{\sigma}{q})^{6}]$) have found that the conductivity diverges with system size although there are disagreements as to whether the divergence is logarithmic or follows a power law behavior [15, 16].

More recently, the combination of disorder and nonlinearity with on-site pinning in one dimensional systems has been considered and molecular dynamical simulations indicate that finite conductivity is obtained [34]. This result naturally raises an interesting question (and the one we will study) as to whether any arbitrarily small nonlinearity is sufficient to destroy the localization caused by the disorder in one dimensional pinned systems.

As with any theory in physics, the best vindication of a theoretical or a numerical result is experimental confirmation. Although Fourier's Law is empirically valid in three-dimensions, it has not been carefully tested in lower dimensional systems. Fortunately, the advances in nanotechnology, and particularly the development of nanotubes, allows a more thorough investigation of the system size dependence of conductivity. The experiments that have been carried out in Single Walled Carbon Nantobues (SWCNT) does point to anomalous heat transport in one-dimension [17, 42]. In another experiment on Multi-Walled Carbon Nanotubes (MWCNT), the conductivity was found to have a power law dependence on the length [19].

1.2 Models Studied/Dissertation Layout

The selection of models we have investigated and whose details and results are described in the rest of this manuscript vary significantly from each other in terms of their qualitative features and the analysis carried out to study them. These were chosen less because they presented a natural transition from one to another, but more because in each case, there was much we needed to understand about the system.

Despite the dissimilarities between them, there are some common elements that we shall briefly state. Except for one set of simulations and results that was generalized to two dimensions, all the models we have considered here are one dimensional. The Hamiltonian for these chains consist of nearest neighbor interactions and, with or without, an external pinning at every site. In the simulations, the chain is subjected to a thermal gradient by attaching the first and last particle to heat reservoirs at unequal temperatures (which is modeled by a Langevin thermal bath).

The following chapters in this manuscript have been organized according to the basic type of dynamics obeyed by the systems that are studied:
In Chapter 2, we look at the alternating mass harmonic chain. Numerical computations indicated that the temperature profile oscillates between two values, and the current depends on whether the total number of particles is even or odd. We derive an exact analytic expression for both the current and the temperature profile in the limit $N \to \infty$. Numerical simulations carried out in a two dimensional alternating mass lattice reveal similar oscillations.

In Chapter 3 we consider a harmonic chain with stochastic dynamics that generates velocity flip at every site. We demonstrate a mapping of pair correlation functions at steady state to that of the self-consistent reservoir model, and use the correspon-

dence to derive the conductivity in the ordered case. Further, the same expression is obtained using the Green-Kubo formula that determines the conductivity from the equilibrium current correlations.

For the pinned disordered system, we use exact numerics to demonstrate (a)finite conductivity at sufficiently large values of N (b) the dependence of the conductivity on the stochastic strength λ and (c) the dependence of conductivity on the disorder strength and pinning. From a theoretical perspective, the Green-Kubo formula is used to establish bounds on the conductivity for disordered systems. For the unpinned chain, we consider two cases, one with boundary pinning and the other with free boundary conditions. We carry out large sets of simulations and demonstrate that the conductivities are the same regardless of the boundary condition, as $N \to \infty$. We address the interesting question of what happens to the conductivity as $\lambda \to 0$?

Finally, we use exact numerics to compute the four-variable correlation functions and show that the steady state is not Gaussian, unlike the system with self-consistent reservoirs. Performing hydrodynamical scaling of the system and applying the large deviation theory an expression is obtained for the fluctuations in the total energy for the ordered system. We carried out careful numerical simulations to verify this result for both pinned and unpinned cases.

In Chapter 4, we turn to nonlinear systems with stochastic noise. The anharmonicity is introduced by a quartic term in the pinning potential and the noise is generated by velocity flips at individual sites. We study the variation of the current (and conductivity) with the size of the system, the strength of anharmonicity and stochasticity. Our data for the ordered masses suggests that both nonlinearity and noise complement each other in obstructing the ballistic transport of phonons and therefore reducing

the current. We also use the data obtained to test an expression that was obtained for the first order correction (in nonlinear coupling strength) to the conductivity. For the range of parameter values we considered, the first order expansion could not account for our results.

The disordered system with both anharmoncitiy and stochastic noise is of great interest because of its potential to shed light on the open question of whether any non-zero anharmonicity can destroy the localization produced by disorder. A very large number of simulations were run in trying to explore this question but obtaining reliable and consistent data in certain parameter regimes proved difficult and our results were unable to resolve the issue.

In the last chapter, we briefly study the effect of introducing a defect in an otherwise ordered harmonic chain. The types of irregularities at a single site we study are caused by a different mass value or a velocity-flipping noise or a quartic pinning term. The data for these models was obtained from exact numerics and dynamical simulations. We note features of similarity in the temperature profile and current across the different models and provide heuristic explanation for some of these.

Chapter 2

Pure Harmonic Systems

One of the most elementary and well-studied systems is the nearest neighbor harmonic crystal. We shall for simplicity consider explicitly the 1d chain but indicate the corresponding state of our knowledge about systems with $d > 1$. The Hamiltonian for a one-dimensional chain with nearest neighbor harmonic coupling is given by:

$$H = \frac{1}{2}\sum_{i=1}^{i=N} p_i^2/2m_i + \frac{1}{2}\sum_{i=1}^{N+1} k_1(q_i - q_{i-1})^2 + \frac{1}{2}\sum_{i=1}^{N} k_0 q_i^2 \quad (2.1)$$

$$= \frac{1}{2} p.\mathbf{M}^{-1}.p + \frac{1}{2} q.\mathbf{\Phi}.q \ , \quad (2.2)$$

where $q = (q_1, q_2, \ldots, q_N)$ and $p = (p_1, p_2, \ldots, p_N)$ denote respectively the displacement and momenta of the N particles of the chain with the boundary condition $q_0 = q_{N+1} = 0$. In the second line we have used a compact notation with $\mathbf{M}$ defining the mass matrix and $\mathbf{\Phi}$ the force-matrix. The ends of the chain are coupled to heat reservoirs at temperatures T_L and T_R. $k_1 > 0$ is the interparticle harmonic interaction.

If $k_0 > 0$, the system is pinned (harmonic) at every site and this feature can be physically interpreted as the chain being attached to a substrate.

The heat current between the sites i and $i+1$ is given by $J_N^{i,i+1} = -\frac{1}{2}k_1\langle(q_{i+1} - q_i)(v_i +$

$v_{i+1})\rangle$ and at steady state we have: $J_N^{1,2} = J_N^{2,3} = \cdots J_N^{N-1,N} = J_N$, is satisfied. This can be seen from the fact the equation for the rate of change of the average local energy ϵ_i at any site i is given by:

$$\begin{aligned} \langle \dot{\epsilon_i} \rangle &= \langle J_N^{i-1,i} \rangle - \langle J_{i,i+!}^N \rangle \\ \langle \dot{\epsilon_i} \rangle &= \frac{d}{dt} \langle \epsilon_i \rangle = 0 \end{aligned} \tag{2.3}$$

We are looking to understand how J_N depends on the size of the chain N.

Harmonic systems are amenable to analytic treatment because we can determine the properties of its vibrational spectrum. The vibrational modes of a harmonic crystal are independent and non-interacting. One can understand the heat transport properties of the system by recognizing that each vibrational mode (or, equivalently, the corresponding phonons) carry the heat across the crystal.

2.1 Discussion of Important Results

The basic model of a one-dimensional chain of uniform masses with nearest neighbor harmonic coupling and connected to Langevin heat reservoirs was studied by Lebowitz *et al* [2]. They obtained an exact solution for the non-equilibrium steady state (NESS) probability density. This was used to show that the heat current J_N, reached a finite positive value, as $N \to \infty$. In other words the heat conductivity, $\kappa_N = J_N N$ diverged as N under the same limit. The temperature profile was determined to be uniform in the bulk of the chain with a value that was arithmetic mean of end temperatures (see Fig.2.1). A variation of this model is a chain where the

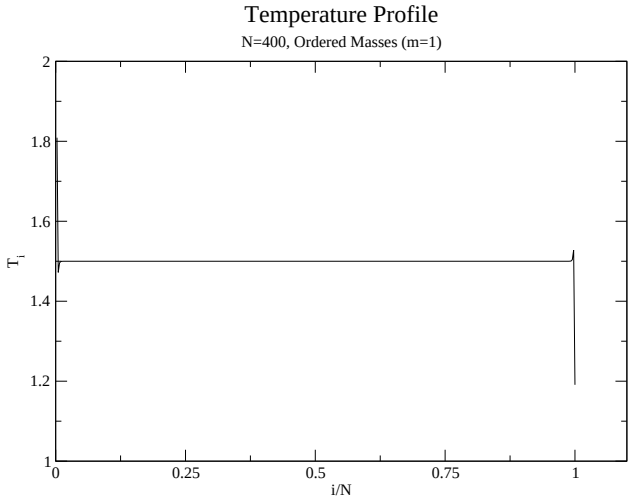

Figure 2.1: Temperature profiles for a chain of uniform masses (m=1) of length 400 and with harmonic nearest neighbor interaction. The ends of the chain are connected to heat reservoirs maintained at temperatures $T_L = 2$ and $T_R = 1$. This system was first analyzed in [2]

arrangement of masses is periodic, i.e, a chain of period C would satisy the condition $m_{i+C} = m_i$ for any pair of sites i, and $i + C$. This configuration also gives infinite conductivity with $\kappa_N \sim N$ [3]. This can be explained in terms of the vibrational modes of the chain, each of which is extended over the entire length of the chain. In the phonon picture, this property translates to phonons propagating freely from one end of the chain to the other. This ballistic transport of phonons implies that the heat transported is independent of the length of the chain (leaving aside the end effects). A similar behavior was shown to be true in higher dimensional crystals [20] , with and without pinning.

2.2 Alternate Mass Chains

We consider the special case of a periodic one-dimensional harmonic chain with the period being two. Let such a chain of length N have masses m_a and m_b. The masses

at the ends of the chain are coupled to temperature reservoirs through the Langevin dynamics.

2.2.1 Governing equations

The equations of motion of the particles is given by:

$$m_i\ddot{q}_i = -\sum_{j=1,N}\Phi_{i,j}q_j + \delta_{i,1}[-\gamma_L\dot{q}_1 + (2\gamma_L T_L)^{1/2}\eta_L] + \delta_{i,N}[-\gamma_R\dot{q}_N + (2\gamma_R T_R)^{1/2}\eta_R]\ , \quad (2.4)$$

for $i = 1, 2, \ldots, N$, where η_L, η_R are Gaussian white noise chosen from distributions with averages $\langle\eta_L(t)\rangle = \langle\eta_R(t)\rangle = 0$ and correlations $\langle\eta_L(t)\eta_L(t')\rangle = \langle\eta_R(t)\eta_R(t')\rangle = \delta(t-t')$ and γ_L, γ_R are dissipation constants.

Corresponding to the Langevin equations in Eq. (2.4) it is straightforward to write the Fokker-Planck equation to describe the evolution of the phase space distribution $\mu(x,t)$, $x = (q_1, \cdots, q_N, p_1, \cdots, p_N)$. Following standard methods [21] it can be shown that the Fokker-Planck equation is given by:

$$\frac{\partial\mu}{\partial t} + \sum_{i=1}^{N}\left[\frac{p_i}{m_i}\frac{\partial\mu}{\partial q_i} - \sum_{j=1}^{N}\Phi_{i,j}q_j\frac{\partial\mu}{\partial p_i}\right] = \sum_{i=1,N}\frac{\gamma_i}{m_i}\frac{\partial}{\partial p_i}\left[p_i\mu + T_i m_i\frac{\partial\mu}{\partial p_i}\right]\ , \quad (2.5)$$

where the right hand side of Eq. (2.5) describes the interaction of the end particles with the heat baths and $T_{1,N} = T_{L,R}$ and $\gamma_{1,N} = \gamma_{L,R}$. Let us define the $2N \times 2N$ matrix

$$\mathbf{a} = \begin{pmatrix} \mathbf{0} & -\mathbf{M^{-1}} \\ \Phi & \mathbf{M^{-1}\Gamma} \end{pmatrix}\ , \quad (2.6)$$

where $\mathbf{\Gamma}$ is a $N \times N$ diagonal matrix with $\Gamma_{ij} = \gamma_i\delta_{ij}(\delta_{i1} + \delta_{iN})$. We also define the $2N \times 2N$ matrix $\mathbf{d}$ with elements $d_{ij} = 2\gamma\delta_{ij}(T_L\delta_{i,N+1} + T_R\delta_{i,2N})$. It is known that

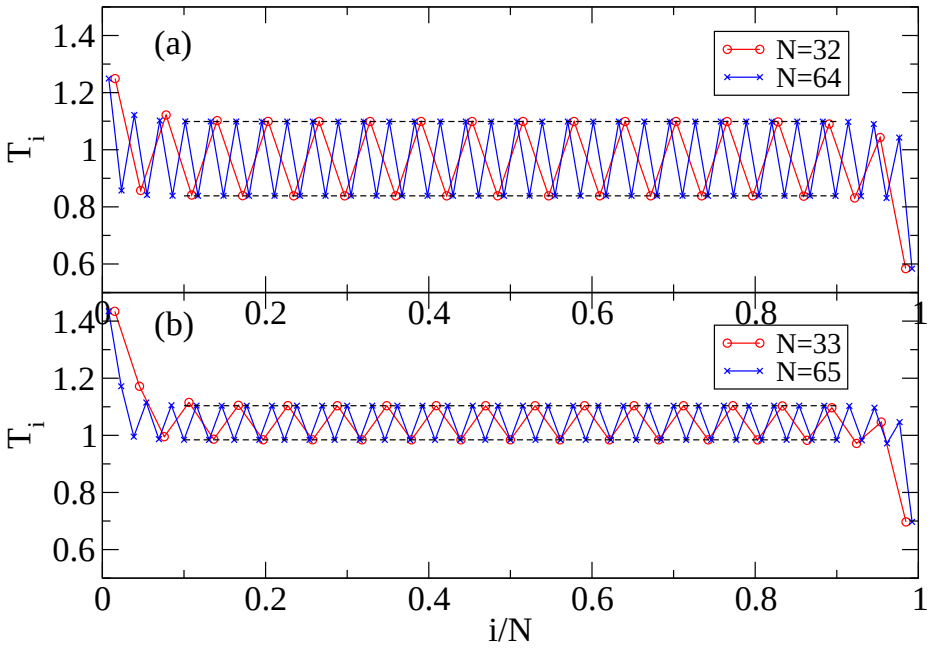

Figure 2.2: Temperature profiles for (a) system with even number of sites $N = 32, 64$, and with $\gamma_L = \gamma_R = 1.0$ and (b) system with odd number of sites $N = 33, 65$, and with $\gamma_L = 1.5, \gamma_R = 0.5$. Other parameters were set to $m_a = 0.75, m_b = 0.25, k = 1, T_L = 1.5, T_R = 0.5$. The mass of the first particle is always taken to be m_a. Note that in (a), the heavier particles are hotter, while in (b), the lighter particles are hotter. The horizontal dashed lines indicate the analytic predictions for $N \to \infty$, from Eqs. (2.24,2.25).

the steady state distribution is Gaussian [2] and given by

$$\mu_s = (2\pi)^{-N} Det[\mathbf{b}]^{-1/2} exp(-\frac{1}{2}\sum_{i,j=1}^{2N} b_{ij}^{-1} x_i x_j) \ ,$$

where the covariance matrix $\mathbf{b}$ with elements $b_{ij} =< x_i x_j >$ satisfies

$$\mathbf{a}.\mathbf{b} + \mathbf{b}.\mathbf{a}^\dagger = \mathbf{d} \ . \tag{2.7}$$

2.2.2 Analytic and numerical results

The solution of the linear equations, Eq.(2.7), gives us all the correlations b_{ij} and hence the temperature profile $T_i =< p_i^2 > /m_i = b_{N+i,N+1}/m_i$, and the current, $J = k\langle(q_{i+1} - q_i)p_i/m_i\rangle = k_1(b_{i+1,N+i} - b_{i,N+i})/m_i$. In the equal mass case the covariance matrix for N sites can be obtained in a fairly explicit form [2]. This seems to be difficult for the alternate mass case. However the matrix equations can be solved numerically for small system sizes and we can obtain accurate results for the temperature profile and current for these system sizes. In Fig. 2.2 we show typical temperature profiles for alternate mass chains with even and odd number of sites for particular choices of parameter values and N. We see oscillations in the temperatures of the particles in the bulk in both the even and odd cases, and the amplitude of the oscillations does not seem to change with system size. In the next section, we will obtain expressions for the current and the bulk temperatures and show that the temperature oscillations persist in the $N \to \infty$ limit.

To obtain analytic results in the limit $N \to \infty$ we follow [3] and express the covariances in terms of integrals over frequencies. The integrands involve elements of the following Green's function:

$$\mathbf{G}^+ = [-\mathbf{M}\omega^2 + \mathbf{\Phi} - i\omega\mathbf{\Gamma}]^{-1} \ . \tag{2.8}$$

Here we are interested in the temperature and current and these are given by [3, 4]

$$\begin{aligned} T_i &= \frac{1}{\pi} m_i \left[\gamma_L T_L \int_{-\infty}^{\infty} d\omega\ \omega^2\ |\mathbf{G}^+_{i1}(\omega)|^2 + \gamma_R T_R \int_{-\infty}^{\infty} d\omega\ \omega^2\ |\mathbf{G}^+_{iN}(\omega)|^2 \right]\ ,\ i = 1, 2, \ldots, N \\ J &= \frac{\gamma_L \gamma_R (T_L - T_R)}{\pi} \int_{-\infty}^{\infty} d\omega\ \omega^2\ |\mathbf{G}^+_{1,N}(\omega)|^2\ . \end{aligned} \tag{2.9}$$

We rewrite the above expressions in the following form.

$$\begin{aligned} T_i &= I_i\ T_L + \hat{I}_i\ T_R\ , \\ J &= \frac{\gamma_R}{m_N} (T_L - T_R) I_N\ , \end{aligned}$$

where the

$$I_i = \frac{m_i \gamma_L}{\pi} \int_{-\infty}^{\infty} d\omega\ \omega^2\ |\mathbf{G}^+_{i1}(\omega)|^2\ ,\quad \hat{I}_i = \frac{m_i \gamma_R}{\pi} \int_{-\infty}^{\infty} d\omega\ \omega^2\ |\mathbf{G}^+_{iN}(\omega)|^2 \tag{2.10}$$

are independent of the temperatures T_L and T_R. Now we note that for the equilibrium case $T_L = T_R$, we must have the same temperature at all sites, *i.e* $T_i = T$, and hence deduce the equality $I_i + \hat{I}_i = 1$. Using this fact and defining $T_L = T + \Delta T/2, T_R = T - \Delta T/2$ we can rewrite the equation for the temperature profile in the following form:

$$T_i = T + (I_i - 1/2)\Delta T = T_R + I_i \Delta T. \tag{2.11}$$

We thus only need to evaluate the integral I_i, in the limit $N \to \infty$.

To simplify our calculations, we only consider the unpinned case $k_0 = 0$. It is straightforward to extend the result to the case $k_0 \neq 0$. For clarity, we may set the odd sites to have $m_i = m_a$ and even sites, $m_i = m_b$. Without loss of generality we can rescale time and mass so that $k_1 = 1$ and $m_a + m_b = 1$.

Our task is to evaluate the integral

$$I_i = \frac{m_i \gamma_L}{\pi} \int_{-\infty}^{\infty} d\omega \; \omega^2 \; |\mathbf{G}^+_{i1}(\omega)|^2 \; , \tag{2.12}$$

where $\mathbf{G}^+ = [-\mathbf{M}\omega^2 + \mathbf{\Phi} - i\omega\mathbf{\Gamma}]^{-1}$. We consider the case with $k = 1$. Let us define $\Delta_{l,m}$ as the determinant of the sub-matrix of $[-\mathbf{M}\omega^2 + \mathbf{\Phi} - i\omega\mathbf{\Gamma}]$ that starts from the l^{th} row and column and ends in the m^{th} row and column. We also define $D_{l,m}$ as the determinant of the sub-matrix of $[-\mathbf{M}\omega^2 + \mathbf{\Phi}]$ starting from the l^{th} row and column and ending in the m^{th} row and column. In terms of these one has:

$$\begin{aligned} \mathbf{G}^+_{l,1}(\omega) &= \frac{\Delta_{l+1,N}}{\Delta_{1,N}}, \quad \mathbf{G}^+_{l,N}(\omega) = \frac{\Delta_{1,l-1}}{\Delta_{1,N}} \qquad (2.13) \\ \text{with} \;\; \Delta_{1,l-1} &= D_{1,l-1} - i\omega\gamma_L D_{2,l-1} \\ \Delta_{l+1,N} &= D_{l+1,N} - i\omega\gamma_R D_{l+1,N-1} \\ \Delta_{1,N} &= D_{1,N} - i\omega(\gamma_R D_{1,N-1} + \gamma_L D_{2,N}) - \omega^2 \gamma_L \gamma_R D_{2,N-1} \; . \qquad (2.14) \end{aligned}$$

Let us now define $f(l) = D_{1,2l}$ and $g(l) = D_{1,2l-1}$. These satisfy the recursion relation,

$$\begin{aligned} \begin{bmatrix} f(l) \\ g(l) \end{bmatrix} &= \mathbf{B} \begin{bmatrix} f(l-1) \\ g(l-1) \end{bmatrix} \; , \\ \text{where } \mathbf{B} &= \begin{bmatrix} (2 - m_a\omega^2)(2 - m_b\omega^2) - 1 & -(2 - m_b\omega^2) \\ (2 - m_a\omega^2) & -1 \end{bmatrix} \; , \end{aligned}$$

with the initial condition $f(0) = 1$ and $g(0) = 0$. Hence we get

$$\begin{bmatrix} f(l) \\ g(l) \end{bmatrix} = \mathbf{B}^l \begin{bmatrix} 1 \\ 0 \end{bmatrix} \; . \tag{2.15}$$

The matrix $\mathbf{B}$ has unit determinant and can be expressed in terms of the Pauli spin

matrices $\vec{\sigma}$ as follows:

$$\begin{aligned} \mathbf{B} &= \cos q\ \mathbf{1} + \imath\vec{\boldsymbol{\sigma}}.\vec{n}\sin q = e^{\imath\vec{\boldsymbol{\sigma}}.\vec{n}q} \\ \text{where } \cos q &= \mathrm{Tr}\frac{\mathbf{B}}{2} = \frac{(2-m_a\omega^2)(2-m_b\omega^2)-2}{2}\ , \end{aligned} \tag{2.16}$$

and $\vec{n}$ is a three dimensional unit vector. Hence we get:

$$\mathbf{B}^l = = e^{\imath\vec{\boldsymbol{\sigma}}.\vec{n}\ lq} = \cos(lq)\ \mathbf{1} + \sin(lq)\frac{\mathbf{B}-\cos q\ \mathbf{1}}{\sin q} \tag{2.17}$$

Combining Eq. (2.17) and Eq. (2.15) we have :

$$f(l) = \frac{\sin(l+1/2)q}{\sin(q/2)} \tag{2.18}$$

$$g(l) = \frac{\sin(lq)}{\sin q}(2-m_a\omega^2) \tag{2.19}$$

Note that for odd-dimensional matrices with the first mass equal to m_b, the determinant would be given by Eq. (2.19) with m_a replaced by m_b. Using these expressions in Eqs. (2.13,2.14), we then get the following forms for the integrals I_i, depending on whether N is even or odd. **Case(1)** - even N:

$$\begin{aligned} I_{odd\ i} &= \frac{2m_a\gamma_L}{\pi}\int_0^\infty d\omega\omega^2 \frac{\left(\frac{\sin^2\frac{(N-i+1)q}{2}}{\sin^2 q}(2-m_b\omega^2)^2 + \gamma_R^2\omega^2\frac{\sin^2\frac{(N-i)q}{2}}{\sin^2(q/2)}\right)}{|\Delta_{1,N}|^2}\ , \\ I_{even\ i} &= \frac{2m_l\gamma_L}{\pi}\int_0^\infty d\omega\omega^2 \frac{\frac{\sin^2\frac{(N-i+1)q}{2}}{\sin^2(q/2)} + \gamma_R^2\omega^2\frac{\sin^2\frac{(N-i)q}{2}}{\sin^2 q}(2-m_a\omega^2)^2}{|\Delta_{1,N}|^2}\ , \\ I_N &= \frac{2\gamma_L m_a}{\pi}\int_0^\infty d\omega\frac{\omega^2}{|\Delta_{1,N}|^2}\ , \end{aligned} \tag{2.20}$$

where

$$\Delta_{1,N} = \left[\frac{\sin\frac{(N+1)q}{2}}{\sin(q/2)} - \gamma_L\gamma_R\omega^2\frac{\sin\frac{(N-1)q}{2}}{\sin(q/2)}\right] + \imath\omega\Big[\gamma_L(2-m_b\omega^2) + \gamma_R(2-m_a\omega^2)\Big]\frac{\sin(Nq/2)}{\sin q}\ .$$

Case(2) - odd N:

$$
\begin{aligned}
I_{odd\ i} &= \frac{2m_a\gamma_L}{\pi}\int_0^\infty d\omega\omega^2 \frac{\left(\frac{\sin^2\frac{(N-i+1)q}{2}}{\sin^2(q/2)} + \gamma_R^2\omega^2(2-m_b\omega^2)^2\frac{\sin^2\frac{(N-i)q}{2}}{\sin^2(q)}\right)}{|\Delta_{1,N}|^2}\ , \\
I_{even\ i} &= \frac{2m_l\gamma_L}{\pi}\int_0^\infty d\omega\omega^2 \frac{(2-m_a\omega^2)^2\frac{\sin^2\frac{(N-i+1)q}{2}}{\sin^2 q)} + \gamma_R^2\omega^2\frac{\sin^2\frac{(N-i)q}{2}}{\sin^2(q/2)}}{|\Delta_{1,N}|^2}\ , \\
I_N &= \frac{2\gamma_L m_a}{\pi}\int_0^\infty d\omega \frac{\omega^2}{|\Delta_{1,N}|^2}\ , \qquad (2.21)
\end{aligned}
$$

where

$$
\Delta_{1,N} = \left[(2-m_a\omega^2)\frac{\sin\frac{(N+1)q}{2}}{\sin q} - \gamma_L\gamma_R\omega^2(2-m_b\omega^2)\frac{\sin\frac{(N-1)q}{2}}{\sin q}\right] + \imath\omega\Big(\gamma_L+\gamma_R\Big)\frac{\sin(Nq/2)}{\sin q}\ .
$$

We now consider points in the bulk such that $x = i/N$ and $(N-i)/N$ remain finite in the $N\to\infty$ limit. We now note that, for real values of $0 < q < \pi$, Eq. (2.16) has two allowed solutions for ω, namely:

$$
\begin{aligned}
\omega_-^2 &= \frac{1}{m_a m_b}[1-\phi(q)] \\
\omega_+^2 &= \frac{1}{m_a m_b}[1+\phi(q)]\ , \\
\text{where } \phi(q) &= [1-2m_a m_b(1-\cos q)]^{1/2}\ ,\ ,0\le q\le\pi\ .
\end{aligned}
$$

These correspond to the frequencies in the acoustic and optical branches of the lattice with the frequency ranges $0 < \omega_- < \sqrt{2/M}$ and $\sqrt{2/m} < \omega_+ < \sqrt{2/(mM)}$, where m (M) is the smaller (larger) of the two masses. For frequencies outside these ranges, Eq. (2.16) gives imaginary values of q. This means that, for these frequencies, terms such as $\sin Nxq$ grow exponentially with N. Hence it is clear that, in the limit $N\to\infty$, the integrals in Eqs. (2.20,2.21) only get contributions from frequencies in

the acoustic and optical bands. Thus for each of the integrals above, we get:

$$\begin{aligned}\int_0^\infty d\omega F(\omega) &= \int_0^{\sqrt{2/M}} d\omega_- \; F(\omega_-) + \int_{\sqrt{2/m}}^{\sqrt{2/(mM)}} d\omega_+ \; F(\omega_+) \\ &= \int_0^\pi dq \Big|\frac{d\omega_-}{dq}\Big| \; F(\omega_-(q)) + \int_0^\pi dq \Big|\frac{d\omega_+}{dq}\Big| \; F(\omega_+(q))\end{aligned}$$

We now note from Eqs. (2.20,2.21) that the required integrands $F(\omega)$ have factors of the form $\sin^2(Nxq)$ in the numerators and $\Delta_{1,N}$ in the denominators. In the limit $N \to \infty$ the factors $\sin^2(Nxq)$ in the numerators can be replaced by $1/2$. Next we note that the determinant $\Delta_{1,N}$ always has the following form:

$$\Delta_{1,N} = A(q)\sin(Nq) + B(q)\cos(Nq) \; , \tag{2.22}$$

where A and B are smooth complex-valued functions. We now obtain the following result for any function $g(\theta, \phi)$ which is periodic in both variables:

$$\begin{aligned}\lim_{N\to\infty} \int_0^\pi \; d\theta \;\; g(\theta, N\theta) &= \lim_{N\to\infty} \frac{1}{N} \int_0^{2\pi(N/2)} d\phi g(\frac{\phi}{N}, \phi) \\ &= \lim_{N\to\infty} \frac{1}{N} \sum_{i=1}^{i=(N/2)} \int_{2\pi(i-1)}^{2\pi i} d\phi g(\frac{\phi}{N}, \phi) = \lim_{N\to\infty} \frac{1}{N} \sum_{i=1}^{i=(N/2)} \int_0^{2\pi} d\psi g(\frac{2\pi(i-1)+\psi}{N}, \psi) \\ &= \lim_{N\to\infty} \sum_{i=1}^{i=(N/2)} \frac{1}{N} \int_0^{2\pi} d\psi g(\frac{2\pi(i-1)}{N}, \psi) = \frac{1}{2\pi} \int_0^\pi d\theta \int_0^{2\pi} d\psi g(\theta, \psi) \; .\end{aligned}$$

Using this we obtain:

$$\begin{aligned}\int_0^\pi dq \frac{C(q)}{|A(q)\sin(Nq) + B(q)\cos(Nq)|^2} &= \int_0^\pi C(q) dq \frac{1}{2\pi} \int_0^{2\pi} d\psi \frac{1}{|A(q)\sin\psi + B(q)\cos\psi|^2} \\ &= \int_0^\pi dq \frac{C(q)}{|A(q)B^*(q) - A^*(q)B(q)|} \end{aligned} \tag{2.23}$$

Using this we get the asymptotic forms of the various integrals in Eqs. (2.20,2.21), and these lead to the results

Case (1)- $N = 2L$, $L \to \infty$:

$$\begin{aligned}
T_o^E &= T + \Delta T \left[\int_0^\pi dq \frac{\gamma_L m_a}{2\pi\phi(q)} \frac{(m_b\omega_+^2 - 2)^2 + 4\gamma_R^2\omega_+^2 \cos^2(q/2)}{|2(\gamma_L+\gamma_R) - (m_a\gamma_R + m_b\gamma_L)\omega_+^2|\ (1+\gamma_L\gamma_R\omega_+^2)} \right. \\
&\quad \left. + \int_0^\pi dq \frac{\gamma_L m_a}{2\pi\phi(q)} \frac{(m_b\omega_-^2 - 2)^2 + 4\gamma_R^2\omega_-^2 \cos^2(q/2)}{|2(\gamma_L+\gamma_R) - (m_a\gamma_R + m_b\gamma_L)\omega_-^2|\ (1+\gamma_L\gamma_R\omega_-^2)} - \frac{1}{2} \right] , \\
T_e^E &= T + \Delta T \left[\int_0^\pi dq \frac{\gamma_L m_b}{2\pi\phi(q)} \frac{4\cos^2(q/2) + \gamma_R^2\omega_+^2(m_a\omega_+^2 - 2)^2}{|2(\gamma_L+\gamma_R) - (m_a\gamma_R + m_b\gamma_L)\omega_+^2|\ (1+\gamma_L\gamma_R\omega_+^2)} \right. \\
&\quad \left. + \int_0^\pi dq \frac{\gamma_L m_b}{2\pi\phi(q)} \frac{4\cos^2(q/2) + \gamma_R^2\omega_-^2(m_a\omega_-^2 - 2)^2}{|2(\gamma_L+\gamma_R) - (m_a\gamma_R + m_b\gamma_L)\omega_-^2|\ (1+\gamma_L\gamma_R\omega_-^2)} - \frac{1}{2} \right] , \\
J^E &= \Delta T \left[\int_0^\pi dq \frac{\gamma_L\gamma_R}{\pi\phi(q)} \frac{\sin^2 q}{|2(\gamma_L+\gamma_R) - (m_a\gamma_R + m_b\gamma_L)\omega_+^2|\ (1+\gamma_L\gamma_R\omega_+^2)} \right. \\
&\quad \left. + \int_0^\pi dq \frac{\gamma_L\gamma_R}{\pi\phi(q)} \frac{\sin^2 q}{|2(\gamma_L+\gamma_R) - (m_a\gamma_R + m_b\gamma_L)\omega_-^2|\ (1+\gamma_L\gamma_R\omega_-^2)} \right] , \qquad (2.24)
\end{aligned}$$

where the subscript o refers to odd sites and e to even sites.

Case (2)- $N = 2L + 1$, $L \to \infty$.

$$\begin{aligned}
T_o^O &= T + \Delta T \left[\int_0^\pi dq \frac{\gamma_L m_a}{2(\gamma_L+\gamma_R)\pi\phi(q)} \frac{4\cos^2(q/2) + \gamma_R^2\omega_+^2(m_b\omega_+^2 - 2)^2}{|(m_a\omega_+^2 - 2) + \gamma_L\gamma_R\omega_+^2(m_b\omega_+^2 - 2)|} \right. \\
&\quad \left. + \int_0^\pi dq \frac{\gamma_L m_a}{2(\gamma_L+\gamma_R)\pi\phi(q)} \frac{4\cos^2(q/2) + \gamma_R^2\omega_-^2(m_b\omega_-^2 - 2)^2}{|(m_a\omega_-^2 - 2) + \gamma_L\gamma_R\omega_-^2(m_b\omega_-^2 - 2)|} - \frac{1}{2} \right] , \\
T_e^O &= T + \Delta T \left[\int_0^\pi dq \frac{\gamma_L m_b}{2(\gamma_L+\gamma_R)\pi\phi(q)} \frac{(m_a\omega_+^2 - 2)^2 + 4\gamma_R^2\omega_+^2 cos^2(q/2)}{|(m_a\omega_+^2 - 2) + \gamma_L\gamma_R\omega_+^2(m_b\omega_+^2 - 2)|} \right. \\
&\quad \left. + \int_0^\pi dq \frac{\gamma_L m_b}{2(\gamma_L+\gamma_R)\pi\phi(q)} \frac{(m_a\omega_-^2 - 2)^2 + 4\gamma_R^2\omega_-^2 cos^2(q/2)}{|(m_a\omega_-^2 - 2) + \gamma_L\gamma_R\omega_-^2(m_b\omega_-^2 - 2)|} - \frac{1}{2} \right] , \\
J^O &= \Delta T \left[\int_0^\pi dq \frac{\gamma_L\gamma_R}{(\gamma_L+\gamma_R)\pi\phi(q)} \frac{sin^2 q}{|(m_a\omega_+^2 - 2) + \gamma_L\gamma_R\omega_+^2(m_b\omega_+^2 - 2)|} \right. \\
&\quad \left. + \int_0^\pi dq \frac{\gamma_L\gamma_R}{(\gamma_L+\gamma_R)\pi\phi(q)} \frac{sin^2 q}{|(m_a\omega_-^2 - 2) + \gamma_L\gamma_R\omega_-^2(m_b\omega_-^2 - 2)|} \right] . \qquad (2.25)
\end{aligned}$$

When $\gamma_L = \gamma_R = \gamma$, we can explicitly carry out the integrals appearing in these expressions and we get the following results.

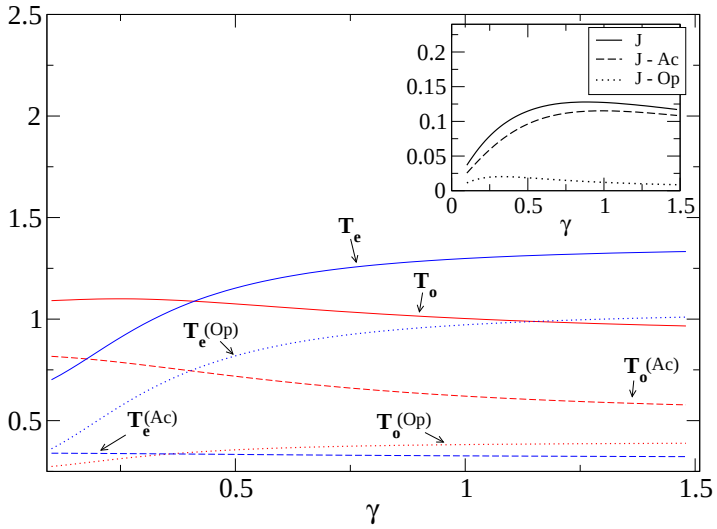

Figure 2.3: Temperatures at odd and even sites for a chain with even number of particles, plotted as a function of $\gamma = \gamma_L = \gamma_R$, $m_a = 0.75, m_b = 0.25, k = 1, T_L = 1.5, T_R = 0.5$. We also plot separately the contributions of the acoustic and optical modes to the temperature at any site. The inset shows J and also the contributions of the acoustic and optical modes.

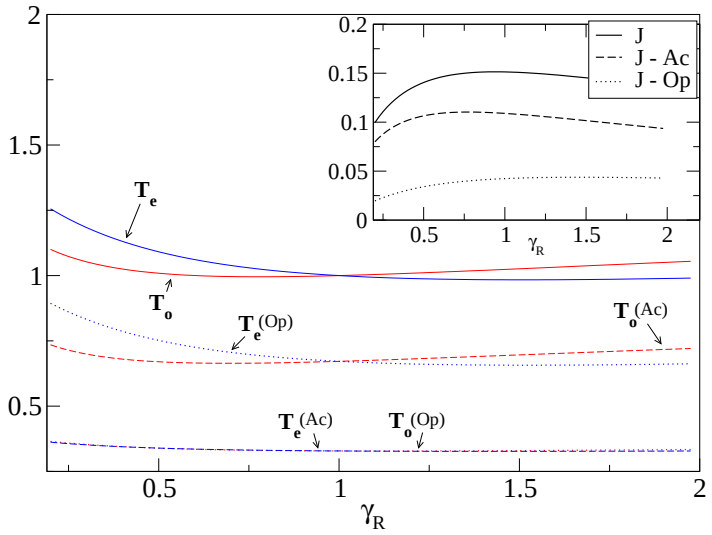

Figure 2.4: Temperatures at odd and even sites for a chain with odd number of particles, plotted as a function of γ_R with $\gamma_L = 1$, $m_a = 0.75, m_b = 0.25, k = 1, T_L = 1.5, T_R = 0.5$. We also plot separately the contributions of the acoustic and optical modes to the temperature at any site. The inset shows the variation of heat current with γ_R and also the contributions of the acoustic and optical modes.

Case (1) - even N:

$$\begin{aligned} I_{odd} &= \frac{m_b}{2}\frac{2(1+\beta)+(\delta^2+2\delta)2\beta+2\frac{\beta^2}{1+2\beta\mu}\delta^2(\delta+1)^2}{\sqrt{2\beta+1}\sqrt{1+2\beta+2\beta^2\mu}} - 4\frac{m_a}{1+2\beta\mu}\left(\sqrt{\frac{1+2\beta+2\beta^2\mu}{1+2\beta}}-1\right) \\ &+ \frac{m_b}{2}\frac{|\delta|(\delta+1)^2}{\mu(1+2\beta\mu)\sqrt{1+\delta^2}} + m_a\frac{2\beta\mu}{1+2\beta\mu}\left(1-\frac{|\delta|}{\sqrt{1+\delta^2}}\right) \qquad (2.26) \\ I_{even} &= m_a\left(1+\frac{-(1+\beta)+\beta(2\delta-\delta^2)-\delta^2(1-\delta)^2\frac{\beta^2}{1+2\beta\mu}}{\sqrt{1+2\beta}\sqrt{1+2\beta+2\beta^2\mu}}+\beta\frac{|\delta|(1-\delta)^2}{\sqrt{1+\delta^2}(1+2\beta\mu)}\right) \\ &+ \frac{m_b}{1+2\beta\mu}\left(-\frac{|\delta|}{\sqrt{1+\delta^2}}+\frac{\sqrt{1+2\beta+2\beta^2\mu}}{\sqrt{1+2\beta}}\right) \qquad (2.27) \\ J^E &= \Delta T\frac{\gamma}{\beta^2\mu(1+4\gamma^2)}[2\beta+1+2\beta^2\mu(1+\delta^2-|\delta|\sqrt{1+\delta^2})-\sqrt{(2\beta+1)(2\beta+1+2\beta^2\mu)}] \qquad (2.28) \end{aligned}$$

where $\mu = 2m_a m_b$, $\delta = m_a - m_b$, $\beta = \gamma^2/(m_a m_b)$.

Case (2) - odd N:

$$\begin{aligned} I_{odd} &= I_{even} = \frac{1}{2}\ , \qquad (2.29) \\ J^O &= \Delta T\frac{\gamma B}{G^2}\left(1-\frac{\sqrt{(F+H)^2-G^2}+\sqrt{(F-H)^2-G^2}}{2F}\right) \qquad (2.30) \end{aligned}$$

where

$$\begin{aligned} F &= \frac{B}{2C}(B^2-4AC)^{1/2}\ , \quad G = C\mu\ , \quad H = \frac{B^2}{2C}-C(1-\mu)-A \\ \text{and} \quad A &= \frac{\delta}{m_b}-\frac{\delta\beta}{m_a}\ , \quad B = \frac{1}{m_b}+\frac{2m_b\beta}{m_a}\ , \quad C = \frac{\beta}{m_a}\ . \end{aligned}$$

2.2.3 Analysis

We now perform some analysis to better understand the physics contained in the expressions we have obtained for even N and odd N for various parameter sets. When $\gamma_L \neq \gamma_R$, we evaluated the integrals in Eqs. (2.24, 2.25) numerically (using Mathematica).

Case (1): We consider chains with even N and set $\gamma_L = \gamma_R = \gamma$. In Fig.2.3 we plot the temperatures on the odd (T_o^E) and even (T_e^E) sites, and also the current (J^E in inset) as a function of the parameter γ. We also separately plot the contributions of the acoustic and optical modes to the temperatures and current. We note the following features:

(i) Depending on the value of γ, either the heavier particles (those on odd sites), or the lighter ones are hotter. At $\gamma \approx 0.41$, the temperatures at the odd and even sites are equal.

(ii) The temperature of the heavier particles gets its main contribution from the acoustic modes while that of the lighter particles comes mostly from the optical modes. The heat current is mostly carried by the acoustic modes.

Case (2): We consider chains with odd N. In this case, $\gamma_L = \gamma_R$ becomes a very special case: the masses of the end particles being equal, this condition implies symmetry between the left and right reservoirs, and this leads to a uniform bulk temperature equal to $(T_L + T_R)/2$. The more typical situation is when the two couplings are different and we consider this by setting $\gamma_L = 1$ and changing γ_R. In Fig. 2.4 we plot the temperatures on the odd (T_o^O) and even (T_e^O) sites, and also the current (J^O in inset) as a function of the parameter γ_R. We also separately plot the contributions of the acoustic and optical modes to the temperatures and current. We note the following features:

(i) Depending on the value of γ_R, either the heavier particles (those on odd sites), or the lighter ones are hotter. At a special value of $\gamma_R = \gamma_L$, the temperatures at the odd and even sites are the same. They are both equal to the mean temperature $T = 1$.

(ii) As for the even N case, here also we see that the temperature of the heavier particles gets it main contribution from the acoustic modes while that of the lighter particles comes mostly from the optical modes. The heat current is again mostly

carried by the acoustic modes.

2.3 Ordered Chain with Single Site Disorder

The system we consider here is the one-dimensional pure harmonic chain with uniform masses everywhere expect at one site. The Hamiltonian for a chain of size N in this case is the given by Eq. (2.2) with the mass matrix $\mathbf{M}$ is a diagonal matrix with all entries being unity expect at site u where it is m_0.

Since the procedure we have described earlier for obtaining the pair correlation in Eq. (2.7) is for a generic configuration of masses, we solve the matrix equation numerically to obtain the temperature profile and the heat current. When the site of disorder, u, is the center of the chain, the steady state temperature profile has two segments: the segment to the left of the of disorder, which has a uniform temperature in the bulk that is closer the left reservoir temperature T_L, and the segment to the right whose uniform temperature is closer to the right reservoir temperature T_R. Around the It is of interest to also look at the chain where the single disorder is created by choosing a different harmonic coupling constant k_0.

2.3.1 Discussion

We have obtained exact expressions for the temperature-profile and the heat current in the alternate mass chain connected to heat baths at different temperatures in the limit of infinite system size. This proves rigorously that the temperature oscillations of successive particles in the bulk persist even in the thermodynamic limit.

We provided an understanding of these oscillations by noting that in any given normal mode, the mean kinetic energy of a particle depends on its mass. In an acoustic mode, the heavier particles have higher mean kinetic energy than the lighter ones, while in an optical mode, the lighter particles have higher kinetic energy. On connecting the

chain to heat reservoirs each of the modes are excited to different degrees, depending on the parameters. The kinetic energy of a particle gets contributions from all the modes, both acoustic and optical and the net result depends on the distribution of energy in the different modes. If both the baths have the same temperature, we have an equilibrium steady state in which each mode has the same average energy (equipartition). In this case the temperature at all sites are equal. The same is true locally when the system is in local equilibrium.

The situation is different in the non-equilibrium case where we do not have local equilibrium and there is no equipartition of energy between the different modes. We then expect generically that the mean kinetic energy (temperatures) obtained by adding the contributions of all modes will depend on the mass of the particle. It is therefore not so surprising that we get different kinetic energies for the different masses. From the above explanation we expect that temperature oscillations should also occur in higher dimensional periodic harmonic systems. Simulation results for two-dimensional strips (see Fig. 2.5) suggest that this is the case, but more extensive studies are necessary to establish the role of dimensionality.

We will return to this problem in a later section 3.4 where we will demonstrate that the oscillations in the bulk will gradually die out when we add anharmonic terms in the Hamiltonian or introduce stochastic noise.

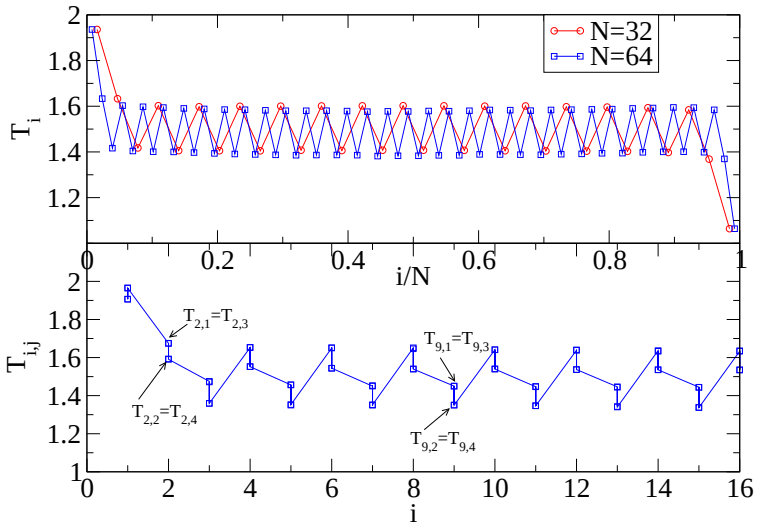

Figure 2.5: Simulation results for temperature profile for a two-dimensional $N \times W$ strip of harmonically coupled particles with a periodic arrangement of masses. The sites on the strip are labeled (i, j) with $i = 1, \ldots, N$ and $j = 1, \ldots, W$. Particles at sites with even $i + j$ have mass m_a and others have masses m_b. Heat baths are attached to all sites on the layers $i = 1$ (temperature T_L) and $i = N$ (temperature T_R). Periodic boundary conditions are imposed in the transverse (j) direction. Upper plot shows the average temperature on successive layers for chains of lengths $N = 32$ and $N = 64$. There are oscillations in the transverse direction also and this is shown in the lower plot which shows the temperatures $T_{i,j}$ on all sites of a section of the $N = 64$ chain. Note that from symmetry we have $T_{i,j} = T_{i,j+2}$, and this can be observed here. The width of the strips were taken to be $W = 4$. The other parameters were taken to be $m_a = 0.6$, $m_b = 1.4$, $\gamma_L = \gamma_R = 1.0$ and $T_L = 2.0, T_R = 1.0$.

Chapter 3

Harmonic systems with bulk noise

3.1 Introduction

We have so far discussed how pure, ordered harmonic systems lead to the heat conductivity, $\kappa \sim N$. This was explained in terms of the ballistic transport of phonons from one reservoir to another. We also noted that this behavior is still true when we consider periodic arrangement of masses or generalize the system to higher dimensions.

It is only natural to ask what happens when we consider a lattice with disordered masses. The vibrational modes of the lattice are found to be localized in such lattices. For one dimensional harmonic chains, it was shown in [3] that this localization leads to a very different form of heat transport. A pinned disordered harmonic chain has a gap in the spectrum and all modes have a finite localization length l and so the current decays exponentially with the size of the system in this situation [24]. For unpinned disordered chains, the low frequency modes are delocalized and hence transport heat [22]. The heat flux now depends on the boundary conditions.

A different dynamics that we can consider is the addition of random noise to the

system. This can be done in several ways, with or without, momentum and energy conservation. The stochastic dynamics results in the scattering of the phonons and this feature alters the transport properties of the system. There has been significantly more success in demonstrating normal conductivity with the addition of stochastic dynamics. In particular, it has been proven that Fourier's Law is obtained for a harmonic chain with energy conserving but momentum non-conserving stochastic perturbation between neighboring sites [26]. Energy and momentum conserving stochastic noise in harmonic chains was considered in [25] and they exhibit normal conductivity in dimension $d \geq 3$.

Another variation of this is the model is a harmonic chain with self-consistent reservoirs [27], where each particle is connected to a Langevin-type heat bath with which it interacts, with the condition imposed that there is no average net transfer of energy between the particle and the internal reservoir. This model with ordered masses was solved exactly and the conductivity was shown to obey Fourier's Law [29].

The system we investigate is a harmonic chain, both ordered and disordered, pinned and unpinned, with a stochastic noise in the bulk. The noise is generated by randomly flipping the velocity of the particles at every site with an average rate λ. We study the system both analytically and using numerical simulations. It is first established that there is a map between the pair correlation functions of the velocity flip model and the self-consistent reservoir model, and the correspondence allows us to demonstrate that Fourier's Law is satisfied for any nonzero flipping rate λ. However, we do not fully understand how the conductivity κ behaves as we take $\lambda \to 0$ for disordered unpinned case. In addition we show a mapping of the steady state equations for one-body and pair-correlation functions to that of the self-consistent reservoirs [27].

3.2 Velocity-Flip Model

The results in this section apply in any dimension. For simplicity of notation we consider here explicitly the one dimensional case; a harmonic chain with the Hamiltonian:

$$\begin{aligned} H &= \sum_{l=1,N}\left[\frac{p_l^2}{2m_l}+k_0\frac{q_l^2}{2}\right]+\sum_{l=2,N}k_1\frac{(q_l-q_{l-1})^2}{2}+k'\left[\frac{q_1^2}{2}+\frac{q_N^2}{2}\right] \\ &= \frac{1}{2}\left[p\hat{M}^{-1}p+q\hat{\Phi}q\right] , \end{aligned} \tag{3.1}$$

where $\{q_l, p_l\}$ denote the position and momenta of the particles. We have used the notation $p = (p_1, p_2, ..., p_N)$, $q = (q_1, q_2, ..., q_N)$ and $\hat{M}$ and $\hat{\Phi}$ are $N \times N$ matrices corresponding to masses and forces respectively. When $k_0 > 0$ we have the pinned case and set $k' = k_1$. In the unpinned case, $k_0 = 0$, we consider fixed, $k' > 0$, and free, $k' = 0$, boundary conditions.

The system's evolution has a deterministic part described by the Hamiltonian above and a stochastic part consisting of two different processes: (i) every particle is subjected to a noise which flips its momentum, *i.e.* for the l^{th} particle the transition $p_l \to -p_l$ occurs with a rate λ, (ii) the particles at the boundaries $l = 1$ and $l = N$ are attached to heat baths with Langevin dynamics at temperatures T_L and T_R respectively. Thus the end particles have additional terms in their equation of motion of the form $-\gamma p_\alpha/m_\alpha + (2\gamma T_\alpha)^{1/2}\eta_\alpha(t)$, for $\alpha = 1, N$, with $\langle \eta_\alpha(t)\eta_{\alpha'}(t')\rangle = \delta_{\alpha,\alpha'}\,\delta(t-t')$, γ is the friction constant and $T_1 = T_L,\ T_N = T_R$ are the bath temperatures.

The master equation describing the time evolution of the full phase space probability density is therefore given by:

$$\frac{\partial P(x)}{\partial t} = \sum_{l,m}\hat{a}_{lm}x_m\frac{\partial}{\partial x_l}P + \sum_{l,m}\frac{\hat{d}_{lm}}{2}\frac{\partial^2 P}{\partial x_l \partial x_m} + \lambda\sum_l[P(..., -p_l, ...) - P(..., p_l, ...)] \tag{3.2}$$

where $x = (q_1, q_2, \ldots, q_N, p_1, p_2, \ldots, p_N) = (x_1, x_2, \ldots, x_{2N})$ and $\hat{a}$ and $\hat{d}$ are $2N \times 2N$

matrices given by:

$$\hat{a} = \begin{pmatrix} 0 & -\hat{M}^{-1} \\ \hat{\Phi} & \hat{M}^{-1}\hat{\Gamma}^{-1} \end{pmatrix} \qquad \hat{d} = \begin{pmatrix} 0 & 0 \\ 0 & 2\hat{T}\hat{\Gamma} \end{pmatrix} . \tag{3.3}$$

Here $\hat{T}$ and $\hat{\Gamma}$ are diagonal matrices with diagonal elements given by $\hat{T}_{ll} = T_L\delta_{l,1} + T_R\delta_{l,N}$ and $\hat{\Gamma}_{ll} = \gamma(\delta_{l,1} + \delta_{l,N})$ respectively. Similar to the case studied in [28] we also find that the equations for the one-body and pair correlation functions of the system are closed. (In fact there are closed equations for each order of the correlation.) We define the vector ρ , $\rho_l =< x_l >$, $l = 1, 2 \ldots 2N$ and the pair correlation matrix

$$\hat{c} = \begin{pmatrix} \hat{u} & \hat{z} \\ \hat{z}^T & \hat{v} \end{pmatrix} . \tag{3.4}$$

where the $N \times N$ matrices $\hat{u}, \hat{z}$ and $\hat{v}$ are given by $\hat{u}_{lm} = \langle q_l q_m \rangle$, $\hat{v}_{lm} = \langle p_l p_m \rangle$ and $\hat{z}_{lm} = \langle q_l p_m \rangle$. It follows then from Eq. (3.2) ρ and $\hat{c}$ satisfy the following equations of motion:

$$\begin{aligned} \frac{d\rho}{dt} &= -\hat{a}\rho + \left(\frac{d\rho}{dt}\right)_{col} , \\ \frac{d\hat{c}}{dt} &= -\hat{a}\hat{c} - \hat{c}\hat{a}^T + \hat{d} + \left(\frac{d\hat{c}}{dt}\right)_{col} , \end{aligned} \tag{3.5}$$

where the last terms in the above two equations arise from the flip dynamics and are given by:

$$\begin{aligned} \left(\frac{d\rho}{dt}\right)_{col} &= -2\lambda \begin{pmatrix} 0 \\ \langle p \rangle \end{pmatrix} \\ \left(\frac{d\hat{c}}{dt}\right)_{col} &= -2\lambda \begin{pmatrix} 0 & \hat{z} \\ \hat{z}^T & 2(\hat{v} - \hat{v}_D) \end{pmatrix} , \end{aligned} \tag{3.6}$$

and $\hat{v}_D$ is a diagonal matrix with matrix elements $[\hat{v}_D]_{ll} = \hat{v}_{ll} = \langle p_l^2 \rangle$.

In the steady state, $d\rho/dt = 0$ which implies $\rho = 0$. Setting $d\hat{c}/dt = 0$ gives the following set of equations for the pair correlations in the NESS:

$$\begin{aligned}
&\hat{z}^T = -\hat{M}\hat{z}\hat{M}^{-1} \ , \\
&\hat{v} = \frac{1}{2}(\hat{M}\hat{u}\hat{\Phi} + \hat{\Phi}\hat{u}\hat{M}) + \frac{1}{2}(\hat{M}\hat{z}\hat{\Gamma}\hat{M}^{-1} + \hat{M}^{-1}\hat{\Gamma}\hat{z}^T\hat{M}) \ , \\
&(\hat{M}\hat{u}\hat{\Phi} - \hat{\Phi}\hat{u}\hat{M}) + (\hat{M}\hat{z}\hat{\Gamma}\hat{M}^{-1} - \hat{M}^{-1}\hat{\Gamma}\hat{z}^T\hat{M}) + 2\lambda(\hat{M}\hat{z} - \hat{z}^T\hat{M}) = 0 \ , \\
&(\Phi\hat{z} + \hat{z}^T\hat{\Phi}) + (\hat{M}^{-1}\hat{\Gamma}\hat{v} + \hat{v}\hat{\Gamma}\hat{M}^{-1}) + 4\lambda(\hat{v} - \hat{v}_D) = 2\hat{T}\hat{\Gamma} \ . \qquad (3.7)
\end{aligned}$$

Using the fact that $\hat{u}$ and $\hat{v}$ are symmetric matrices we have $N^2 + N(N+1)$ unknown variables and there are that many independent equations above.

3.3 Mapping to Self-Consistent Reservoir model

Now consider the case of heat conduction across a harmonic chain with Hamiltonian given by (3.1) and self consistent reservoirs attached to all sites. This is in addition to the two end reservoirs at fixed temperatures T_L and T_R. Each of the side reservoirs is a Langevin bath with a friction constant γ_l' and a temperature T_l', $l = 1, 2, ...N$, which is self-consistently fixed by the condition that there is no net flow of energy into the reservoir [29]. The stochastic equations of motion of this system are:

$$\begin{aligned}
\frac{dp_1}{dt} &= -\Phi_{1m}q_m - \frac{\gamma}{m_1}p_1 - \frac{\gamma_1'}{m_1}p_1 + (2\gamma T_L)^{1/2}\eta_1(t) + (2\gamma_1' T_1')^{1/2}\zeta_1(t) \\
\frac{dp_l}{dt} &= -\Phi_{lm}q_m - \frac{\gamma_l'}{m_l}p_l + (2\gamma_l' T_l')^{1/2}\zeta_l(t) \quad l = 2, ..., N-1 \ , \\
\frac{dp_N}{dt} &= -\Phi_{Nm}q_m - \frac{\gamma}{m_N}p_N - \frac{\gamma_N'}{m_N}p_N + (2\gamma T_R)^{1/2}\eta_N(t) + (2\gamma_N' T_N')^{1/2}\zeta_N(t) \qquad (3.8)
\end{aligned}$$

where η_1, η_N and ζ_l, $l = 1, 2, ..., N$ are independent Gaussian white noise sources with unit variance. It is immediately established that the probability distribution $P(x)$ in

the NESS of this model is a Gaussian. The self consistency condition for zero current into the side reservoirs is given by $T'_l = \hat{v}_{ll} = \langle p_l^2 \rangle / m_l$. Making the identification $\gamma'_l = 2\lambda m_l$ and correspondingly defining $\hat{\Gamma}' = 2\lambda \hat{M}$ and $\hat{T}'$,the diagonal matrix of T'_l, we can see that the equations (3.7) can be rewritten by replacing $\hat{\Gamma}$ by $\hat{\Gamma} + \hat{\Gamma}'$, and $\hat{T}$ by $T \hat{+} T'$, and thus absorb all the factors containing λ. In this form we can immediately see that they are the system of equations for pair-correlations corresponding to the self-consistent model defined above.

This identification allows us to immediately use the result for the conductivity for the ordered case defined in [29] [Eq. 6.7] (with all the masses m_i set to unity).

$$\begin{aligned} \kappa &= \frac{k_1 D}{8\lambda m} , \\ \text{where } D &= \frac{4k_1}{2k_1 + k_0 + [(k_0)(4k_1 + k_0)]^{1/2}} . \end{aligned} \tag{3.9}$$

This is an exact result for the ordered system, but there is no immediate extension using this method, to the disordered case.

3.4 Alternate Mass Chain with Velocity Flip

It should be noted too, that for the alternate mass harmonic chain studied in the earlier section, the addition of stochastic noise reduces the oscillations, and as $N \to \infty$ they decay and we also get regular transport. We briefly discuss this here, under the categories of momentum conserving and momentum non-conserving noise.

(a) *Momentum conserving noise*: Here, in addition to the Hamiltonian dynamics without pinning, one introduces random exchange of momentum between nearest neighbor particles, which occurs with a rate λ. This conserves both momentum and energy. In Figs. 3.1 and 3.2, we show the effect of momentum conserving noise on the temperature profiles for chains of even and odd number of particles. In the even N

case we see that, on introducing noise, the size of the oscillations has decreased and the phase of the oscillation on the left half has changed sign. For the odd case, the choice of parameters ($\gamma_L = \gamma_R = 1$) corresponds to a case with no oscillations when $\lambda = 0$. On introducing noise, $\lambda > 0$, one gets oscillations very similar to the even N case. We also see that the oscillation amplitude becomes smaller on increasing system size, for both even and odd N cases.

Thus we see that the temperature profile in this system with energy-momentum conserving noisy dynamics shows the following qualitative features : (i) The oscillations decay as we go into the bulk, (ii) There is a phase shift in the sign of the oscillation amplitude as one crosses the center of the chain. The lighter particles at the hot end are always hotter than the heavier particles. At the cold end, the heavier particles are hotter. Thus this is *qualitatively* different from the harmonic case, (iii) For large N, the temperature profile is not sensitive to whether N is even or odd.

(b) *Momentum non-conserving case*: In Figs. (3.3,3.4), we show the effect of addition of velocity flipping dynamics on the temperature profile for harmonic chains with odd and even number of particles. We observe that for the even case, the oscillations in the temperature decreases considerably on introducing the noise, and this reduction is greater when N is larger. For the odd case however, for small systems, introduction of noise produces small oscillations in the temperature profile, but these oscillations eventually decrease as the system-size is increased. For both even and odd total number of particles, the decay of the oscillation amplitude with system size is faster than for the momentum-conserving case and we quickly get a linear temperature profile in the bulk of the system.

The rest of the analysis would be focused on understanding the disordered system.

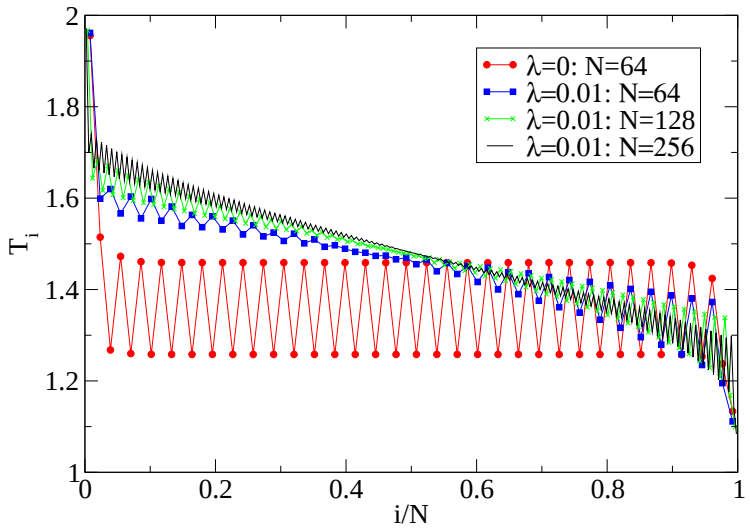

Figure 3.1: Temperature profiles with energy– and momentum–conserving noisy dynamics for a harmonic chain with even number of particles. Other parameters were taken to be $m_a = 0.5$, $m_b = 1.5$, $\gamma_L = \gamma_R = 1.0$ and $T_L = 2.0, T_R = 1.0$.

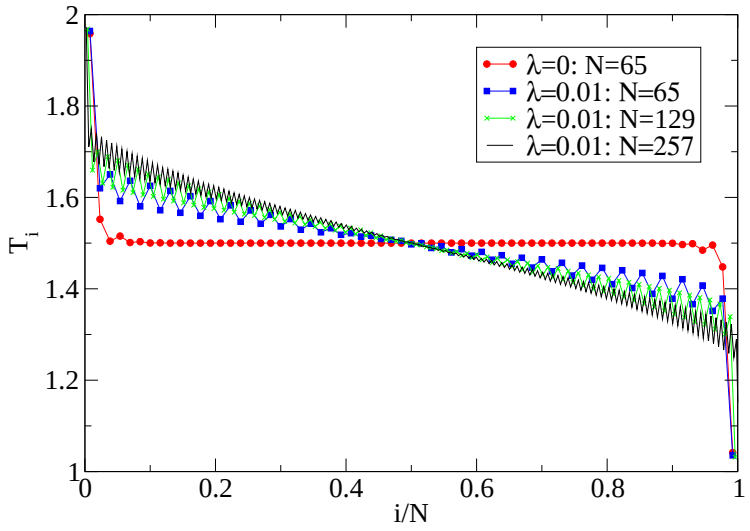

Figure 3.2: Temperature profiles with energy– and momentum–conserving noisy dynamics for a harmonic chain with an odd number of particles. Other parameters were taken to be $m_a = 0.5$, $m_b = 1.5$, $\gamma_L = \gamma_R = 1.0$ and $T_L = 2.0, T_R = 1.0$.

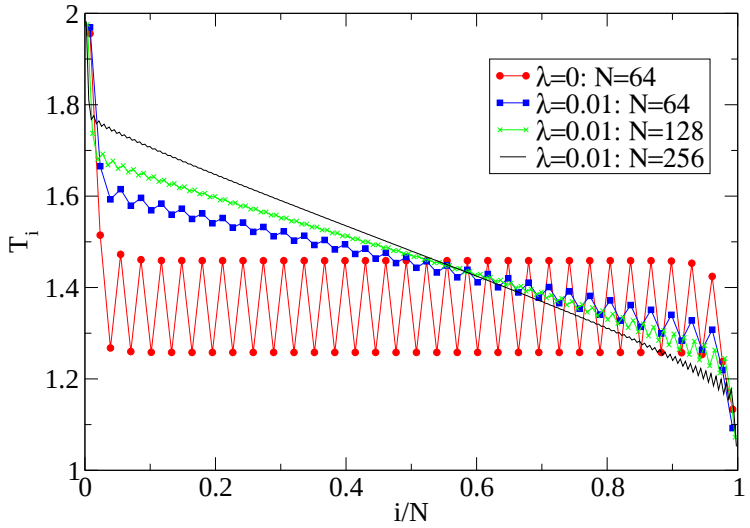

Figure 3.3: Temperature profiles with only energy–conserving noisy dynamics for a harmonic chain with even number of particles. Other parameters were taken to be $m_a = 0.5$, $m_b = 1.5$, $\gamma_L = \gamma_R = 1.0$ and $T_L = 2.0, T_R = 1.0$.

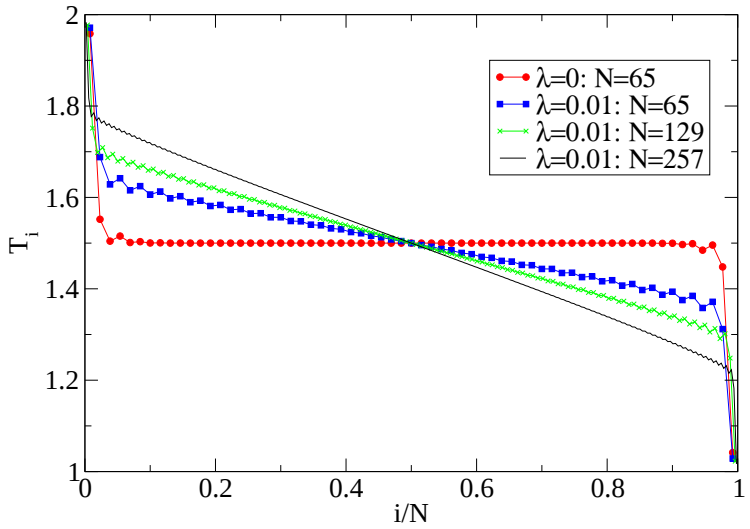

Figure 3.4: Temperature profiles with only energy–conserving noisy dynamics for a harmonic chain with an odd number of particles. Other parameters were taken to be $m_a = 0.5$, $m_b = 1.5$, $\gamma_L = \gamma_R = 1.0$ and $T_L = 2.0, T_R = 1.0$.

3.5 Green-Kubo Formula

An indirect analytical way to calculate the infinite size conductivity (if it exists) is the application of the Green-Kubo formula. This approach is based on the assumption that fluctuations of macroscopic quantities at equilibrium obey the same macroscopic physical laws as the relaxation of the same quantities when they are perturbed out of equilibrium. Accordingly, the expression for the conductivity of a one dimensional system is given by :

$$\kappa_{GK} = \lim_{\tau\to\infty} \lim_{N\to\infty} \frac{1}{k_B T^2} \int_0^\tau \sum_{i=1}^{N} \langle j_{i,i+1}(t) j_{0,1}(0) \rangle \tag{3.10}$$

The very definition implies that the formula applies to the infinite size limit of the system, and the resulting value of the expression would be finite only if the system exhibits regular diffusive transport. There are different derivations of this formula [30], [31].

3.5.1 Bounds from Green-Kubo formula

Bernardin [32] considered a model of a disordered harmonic chain with a stochastic noise that changes the momentum of neighboring particles while keeping the sum of their kinetic energies constant. He obtained an exact result for the Green-Kubo conductivity of an ordered chain and also rigorous upper and lower bounds for the conductivity of disordered chains. Here we use Bernardin's approach for our model to obtain an exact expression for the ordered chain. We also obtain bounds for the conductivity of the disordered chain which are slightly improved from those of Bernardin's.

The time evolution of the phase space density is given by Eq. (3.2) which we rewrite

here in a more abstract form for convenience.

$$\begin{aligned}
\frac{\partial P(x)}{\partial t} &= LP(x) \\
\text{where } L &= A + \lambda S \\
AP(x) &= \sum_{l=1}^{N}[-\frac{p_l}{m_l}\frac{\partial P(x)}{\partial q_l} + \sum_{m=1}^{N}\Phi_{lm}q_m\frac{\partial P(x)}{\partial p_l}] \\
SP(x) &= \sum_{l}[P(...,-p_l,...) - P(...,p_l,...)] \ . \qquad (3.11)
\end{aligned}$$

The total current which is carried entirely by the Hamiltonian part can be written in the following form:

$$\mathcal{J} = \frac{k_1}{2}\sum_{l=1}^{N}\frac{p_l}{m_l}(q_{l+1} - q_{l-1}) \ \ , q_0 = q_N \ , q_{N+1} = q_1. \qquad (3.12)$$

The Green-Kubo expression for the thermal conductivity at temperature T is given by:

$$\begin{aligned}
\kappa_{GK} &= \lim_{z\to 0}\lim_{N\to\infty}\frac{1}{NT^2}\int_0^\infty dt\ e^{-zt}\ \langle \mathcal{J}(0)\mathcal{J}(t)\rangle \\
&= \lim_{z\to 0}\lim_{N\to\infty}\frac{1}{NT^2}\int_0^\infty dt\ e^{-zt}\ \int dx\ \mathcal{J}\ e^{Lt}\ (\ \mathcal{J}\ P_{eq}\ ) \\
&= \lim_{z\to 0}\lim_{N\to\infty}\frac{1}{NT^2}\ \langle\ \mathcal{J},\ (z-L)^{-1}\ \mathcal{J}\ \rangle\ . \qquad (3.13)
\end{aligned}$$

where we have used the notation $\langle f, g\rangle = \int dx f(x)g(x)P_{eq}$ for any two functions f, g of phase space variables $x = (q_1, \ldots, q_N, p_1, \ldots, p_N)$ and $P_{eq} \sim exp[-\beta H]$ where H is given by the periodicized version of Eq. (3.1) with k' set equal to 0.

We note the following relations which are easy to prove:

$$\begin{aligned}
A\mathcal{J}P_{eq} &= \sum_{l,j}\frac{\Phi_{lj}q_j}{m_l}(q_{l+1} - q_{l-1})P_{eq} \\
\text{and} \quad S\mathcal{J}P_{eq} &= -2\mathcal{J}P_{eq} \qquad (3.14)
\end{aligned}$$

Green-Kubo conductivity for equal mass ordered case

For the equal mass case Eq. (3.14) gives $A\mathcal{J}P_{eq} = 0$. This is true with or without pinning and corresponds to the fact that for periodic boundary conditions the current operator commutes with the Hamiltonian. Hence we get:

$$\kappa_{GK} \;=\; \lim_{z\to 0}\lim_{N\to\infty}\frac{1}{T^2N}\int dx\ \mathcal{J}\ \frac{1}{z+2\lambda}\ \mathcal{J}\ P_{eq} = \lim_{N\to\infty}\frac{\langle \mathcal{J}^2\rangle}{2\lambda T^2 N}\ .$$

Using the form of $\mathcal{J}$ in Eq. (3.12) we then get the same result as Eq. (3.9)
In the self-consistent model [29], the conductivity was independent of boundary conditions for the ordered case and while not proven we expect this to be true also for the disordered case for $N \to \infty$ at fixed $\lambda > 0$. In fact there is every reason to believe that whenever the Green-Kubo formula for κ_{GK} converges to a finite value when $N \to \infty$ then it will agree with the conductivity in the NESS defined as $\kappa = \lim_{N\to\infty}\lim_{T_L\to T_R\to T} N\langle J_N\rangle/(T_L - T_R)$.

Upper and lower bounds on the Green-Kubo conductivity

We now consider the random case where the masses are independently chosen from some distribution. Bernardin's proof that the conductivity κ_{GK} is bounded away from zero and infinity is based on an identity between $\langle \mathcal{J}, (z-L)^{-1}\mathcal{J}\rangle$ and a variational expression (Eq (15) in [32]),

$$\langle \mathcal{J}, (z-L)^{-1}\mathcal{J}\rangle = Sup\{2\langle u, J\rangle - \langle (z-\lambda S)u, u\rangle - \langle (z-\lambda S)^{-1}Au, Au\rangle\} \quad (3.15)$$

where the supremum is carried out over the set of smooth functions $u(q,p)$. The derivation of this formula is straightforward for A=0. More generally we can consider a symmetric L, e.g one corresponding to a stochastic dynamics satisfying detailed balance with respect to P_{eq}. Then we have that u is the solution of the equation

$Lu = \mathcal{J}$, and both sides of Eq.(3.15) are equal to $\langle \mathcal{J}, u \rangle$. For a derivation of Eq. (3.15) in the case $L = S + A$ with A antisymmetric, see [33].

Lower bound: Choose a test function $u = \mu \sum_l p_l (q_{l+1} - q_{l-1})$, where μ is a variational parameter:

$$\begin{aligned} \langle u, \mathcal{J} \rangle &= \frac{k\mu T}{2} \sum_l \langle (q_{l+1} - q_{l-1})^2 \rangle = NT^2 \frac{\mu D}{2} \ , \\ \langle (z - \lambda S)u, u \rangle &= (z + 2\lambda)\langle u^2 \rangle = (z + 2\lambda)\mu^2 T \sum_l m_l \langle (q_{l+1} - q_{l-1})^2 \rangle \ . \end{aligned}$$

where D is defined in Eq. (3.9). Denoting by [...] an average over disorder we then get:

$$[\langle (z - \lambda S)u, u \rangle] = NT^2 (z + 2\lambda) \frac{\mu^2 D[m]}{k} \quad .$$

Similarly,

$$\langle (z - \lambda S)^{-1} Au, Au \rangle = (z + 4\lambda)^{-1} \langle (Au)^2 \rangle = (z + 4\lambda)^{-1} \mu^2 T^2 \sum_l \left(\frac{1}{m_l} - \frac{1}{m_{l+1}} \right)^2 m_l m_{l+1} \ ,$$

and averaging over disorder gives

$$\left[\langle (z - \lambda S)^{-1} Au, Au \rangle \right] = 2NT^2 (z + 4\lambda)^{-1} \mu^2 \left([m] \left[\frac{1}{m} \right] - 1 \right) \ .$$

Thus we have:

$$\frac{1}{NT^2} [\langle \mathcal{J}, (z - L)^{-1} \mathcal{J} \rangle] \geq D\mu - C\mu^2 \tag{3.16}$$

$$\text{where} \quad C = \frac{2\lambda D[m]}{k} + \frac{1}{2\lambda} ([m] \left[\frac{1}{m} \right] - 1) \ . \tag{3.17}$$

The minimum of the bound occurs at $\mu = D/(2C)$ and this gives:

$$[\kappa_{GK}] \geq \frac{D^2}{4C} \ . \tag{3.18}$$

Upper bound: By neglecting the last term in Eq. (3.15) which is clearly negative, we get the upper bound:

$$\langle \mathcal{J}, (z-L)^{-1}\mathcal{J}\rangle \ \leq \ (z+2\lambda)^{-1}\langle \mathcal{J}^2\rangle = (z+2\lambda)^{-1}T\frac{k_1^2}{4}\sum_l \frac{1}{m_l}\langle (q_{l+1}-q_{l-1})^2\rangle \tag{3.19}$$

Hence,

$$[\kappa_{GK}] \ = \ \frac{1}{NT^2}\left[\langle \mathcal{J}, (z-L)^{-1}\mathcal{J}\rangle\right] \leq \frac{k_1 D}{8\lambda}[\frac{1}{m}] \ . \tag{3.20}$$

Combining (3.18) and (3.20) gives:

$$\frac{k_1 D}{8\lambda[m](1+k_1\frac{[1/m]-1/[m]}{4\lambda^2 D})} \leq [\kappa_{GK}] \leq \frac{k_1 D}{8\lambda}[\frac{1}{m}] \tag{3.21}$$

As $\lambda \to \infty$, both bounds behave as $1/\lambda$ while for $\lambda \to 0$, the upper bound diverges while the lower bound goes to 0 linearly in λ. The behavior of κ_{GK} and of κ in the NESS when $\lambda \to 0$ after $N \to \infty$ is thus not determined by these bounds and remains an open problem for both the pinned and unpinned random mass case. What we do know is that, if $\lambda \to 0$ with N finite then there is a significant difference between the pinned and unpinned cases [34, 22]. As already noted, all phonon modes are localized for the pinned case with a fixed localization length independent of N and the current decays exponentially with system size. In the unpinned case the low frequency modes are extended and the current has a power law decay with an exponent that depends on the boundary conditions used [22], $\kappa_N \sim N^{-1/2}$ for fixed BCs [3, 35] and as $\kappa_N \sim N^{1/2}$ for free BCs [23, 36]. With the addition of the noisy dynamics which conserves energy but not momentum we expect as noted earlier that the conductivity κ will be equal to κ_{GK} and thus strictly positive for any $\lambda > 0$ [26]. In the following section we evaluate

$\langle J_N \rangle$ as a function of λ and N numerically and via computer simulations, to obtain information about its behavior when $\lambda \to 0$.

3.6 Disordered Masses: Numerics and Simulations

We study the dependence of the heat current in the NESS on the system size and on the strengths of the disorder and noise. In all our computations we set $k = 1$. The masses $\{m_l\}$ are chosen from a uniform distribution between $1 - \Delta$ to $1 + \Delta$. This gives $[m] = 1, [1/m] = 1/(2\Delta) \ln[(1+\Delta)/(1-\Delta)]$. The average heat current from site l to $l + 1$ is given by $j_{l+1,l} = k_1 \langle q_l p_{l+1}/m_{l+1} \rangle$. In the steady state this is independent of l and we denote $j_{l+1,l} = \langle J_N \rangle$. We note that $\langle J_N \rangle = k_1 \hat{z}_{l,l+1}/m_{l+1}$ and hence we can obtain accurate numerical values for the current in the disordered system by solving the equations for the correlation matrix *i.e* Eqs. (3.7). This involves solving large dimensional linear matrix equations and we have been able to do this for system sizes less than $N = 512$. For larger sizes we performed nonequilibrium simulations and obtained the steady state current by a time average. For small sizes we verified that both methods agreed to very high accuracy. The number for disorder realizations was 100 for $N \leq 64$, and varied between $2 - 16$ for larger sizes. The error bars in our data presented below are calculated using the results from different realizations.

3.6.1 Pinned case

This corresponds to the case with $k_0 > 0$ and here we also set $k' = 1$. All results in this section were obtained by numerical solution of Eqs. (3.7). In Fig. 3.5 we plot $\langle J_N \rangle N/\Delta T$ versus N for different values of the flipping rate λ and with $\Delta = 0.8,\ k_0 = 4$. In all cases we see a rapid convergence to a system-size independent value which then gives the conductivity κ of the system. In Fig. 3.6 we plot κ, obtained from the large-N data in Fig. 3.5, as a function of λ. For comparison we also plot the lower

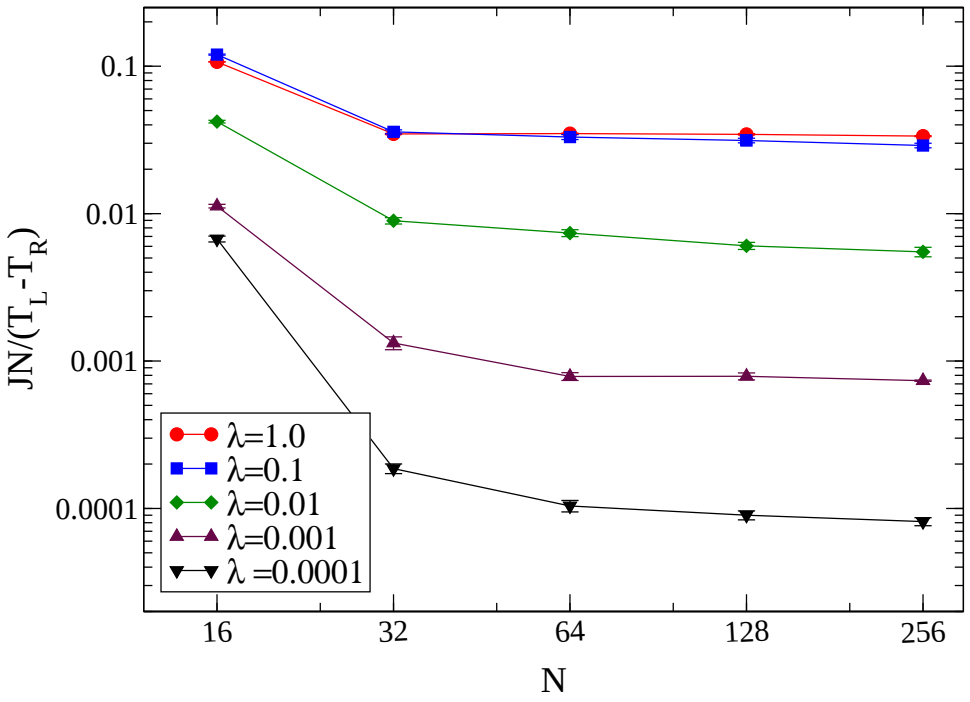

Figure 3.5: Plot of $JN/(T_L - T_R)$ versus N for for different values of λ. The parameter values were set at $k_0 = 4, k = 1, \Delta = 0.8$. All the data shown here were obtained from exact numerical computation.

and upper bounds for the Green-Kubo conductivity given by Eqs. (3.18,3.20). It is seen that κ has a maximum around $\lambda \simeq 0.5$. This can be thought of as a balance between the flips delocalizing the phonons and acting as scatterers of phonons.

In accord with the bounds we find that at large λ, $\kappa \sim 1/\lambda$ while at small λ, the numerical results suggest $\kappa \sim \lambda$. We note that for $\lambda = 0$, all phonon modes are exponentially localized within length-scales $\ell \sim (k_0\Delta^2)^{-1}$. One can argue that for small values of λ there is diffusion of energy between these localized states with a diffusion constant $\sim \ell^2\lambda$. This leads to the $\kappa \sim (k_0^2\Delta^4)^{-1}\lambda$ and we now test this numerically. In Figs. (3.7,3.8) we show the numerical data which suggests the scalings $\kappa \sim \Delta^{-4}$ and $\kappa \sim {k_0}^{-2.5}$, which are roughly consistent with the expected behavior. The reason for the discrepancy could be that we are not yet in the strong localization regime where the prediction is expected to be most accurate.

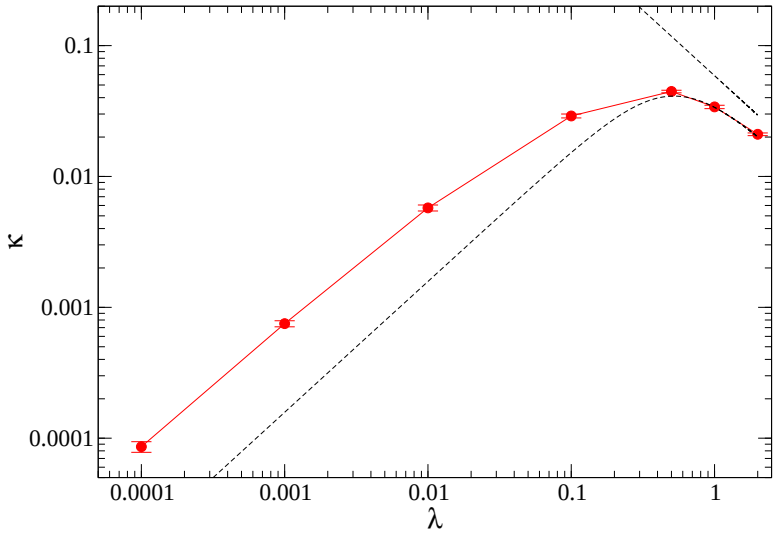

Figure 3.6: Plot of κ versus λ obtained from the numerical data in Fig. 3.5. The lower and upper bounds for κ_{GK} given by Eqs. (3.18,3.20) are shown by the dashed lines.

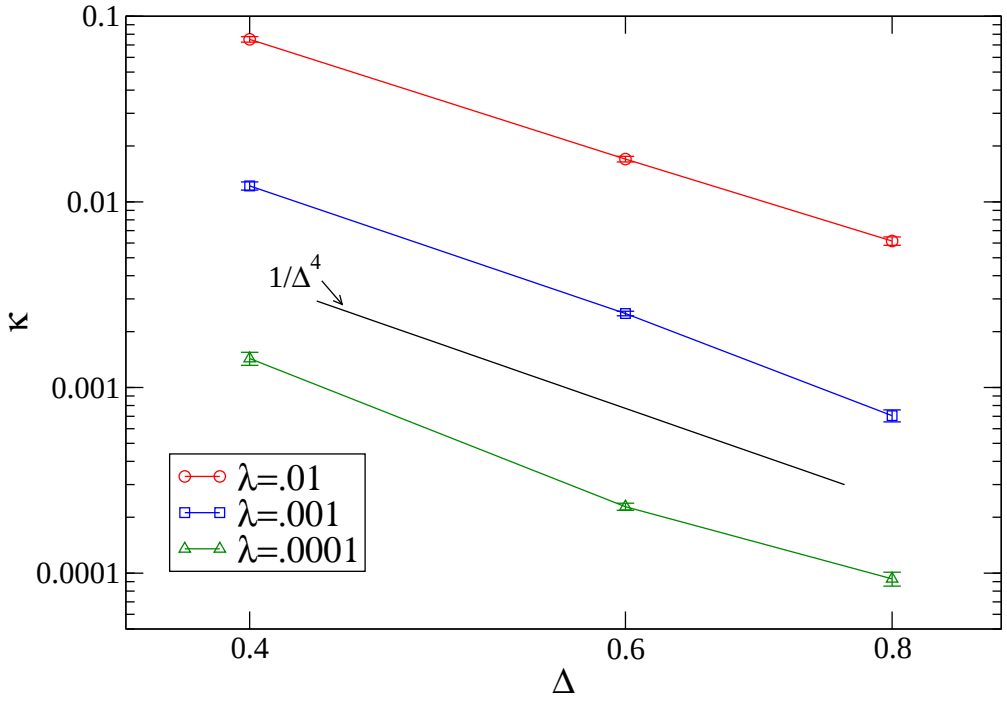

Figure 3.7: Plot of κ versus Δ for different values of λ and with $k_0 = 4$ and $k = 1$. We also show a straight line with slope -4.0.

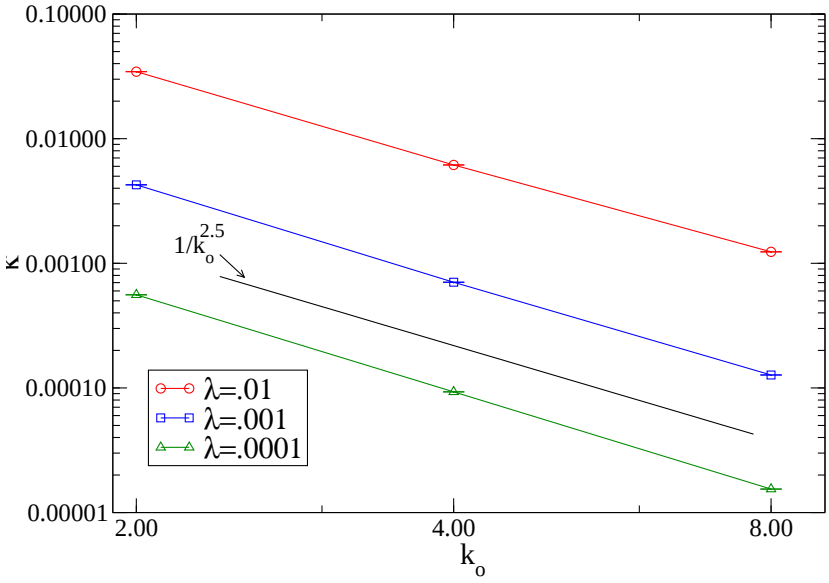

Figure 3.8: Plot of κ versus k_0 for different values of λ and with $\Delta = 0.8$ and $k = 1$. We also show a straight line with slope -2.5.

3.6.2 Unpinned case

As noted above for the unpinned case with $\lambda = 0$, the two different boundary conditions(BC) namely fixed BCs with $k' > 0$ and free BCs with $k' = 0$ give respectively $\langle J_N \rangle \sim N^{-3/2}$ [3] and $\langle J_N \rangle \sim N^{-1/2}$ [23]. The difference in the asymptotic behavior of the current for different BCs can be understood as arising from the dependence on BCs of the transmission of the low frequency modes which carry the current [22]. For any $\lambda > 0$ however we expect that the system should have a unique finite value of the conductivity, independent of boundary conditions, the same as for κ_{GK}. Physically we can argue as follows: The unpinned system without disorder has a finite positive κ given by Eq. (3.9), which is independent of BCs [see comments at end of sec. (3.5.1)]. The low frequency modes are weakly affected by disorder hence we expect that as far as these modes are concerned the unpinned system with and without disorder will

behave similarly. Since these are the modes which led to the dependence on BCs for the case $\lambda = 0$, we expect that for $\lambda > 0$ they will not have any effect.

We now present results of our numerical and simulation studies of the unpinned chain with free and fixed BCs. The numerical results are obtained by solving Eqs. (3.7). The simulation involves evolving the system with the Hamiltonian part, the momentum flips at all sites and the Langevin baths at the boundary sites. For $N \leq 512$, the numerical method was employed to arrive at the solution for the NESS whereas for larger values of N, we performed simulations to obtain the data. In Fig. 3.9 we plot $JN/(T_L - T_R)$ versus N for different values of λ for both fixed and free BCs. The disorder strength is $\Delta = 0.8$. For both BCs we can see flattening of the curves at large system sizes for the parameter values $\lambda = 0.1, 0.01$ implying a finite κ, which is independent of BCs. For $\lambda = 0.001, 0.0001$ it appears that reaching the asymptotic

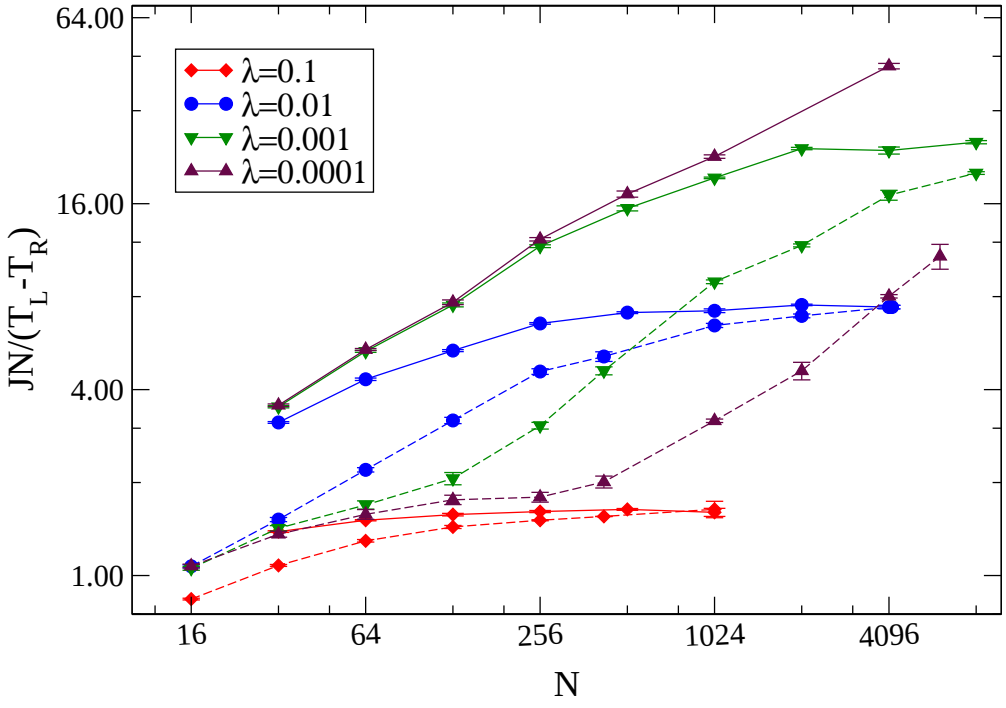

Figure 3.9: Plot of $JN/(T_L - T_R)$ versus N for the unpinned case with both fixed (dashed lines) and free BCs (solid lines) for different values of λ and parameter values $k = 1$ and $\Delta = 0.8$. The data for $N < 512$ were obtained using exact numerics and in all these cases simulations give very good agreement with the numerics. For $N \geq 512$, the data were obtained from simulations alone.

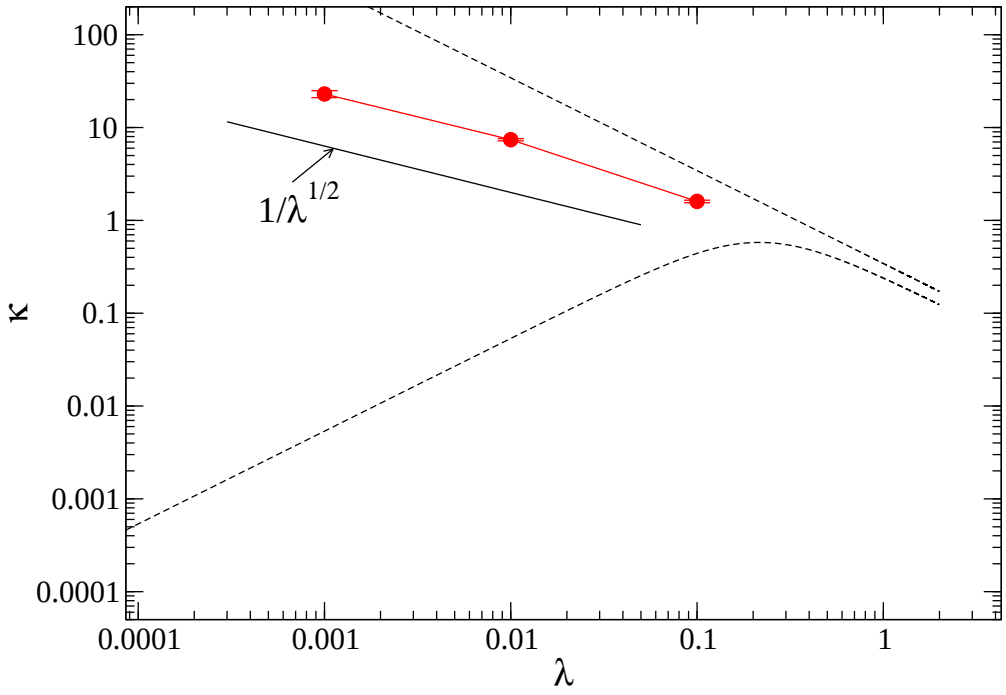

Figure 3.10: Plot of κ versus λ for the unpinned system obtained from the numerical data in Fig. 3.9. The lower and upper bounds for κ_{GK} given by Eqs. (3.18,3.20) are shown by the dashed lines. Also shown is a straight line with slope $-1/2$.

limit requires larger system sizes.

Using the large-N data in Fig. 3.9 we estimate the conductivity $\kappa = JN/\Delta T$ and this is plotted in Fig. 3.10. In Fig. 3.11 we show a typical plot of the temperature profile for the case with fixed BC (this was obtained using exact numerics). The profile is close to linear consistent with the fact that the conductivity is temperature-independent. We do not see any significant boundary temperature jumps since the system size is sufficiently large. In Fig (3.12) we have the profile for N=128 for the case $\lambda \to 0$ which shows considerable jump in the temperatures across neighboring sites.

It appears likely that for all $\lambda > 0$ the conductivity κ is independent of BCs. However this is difficult to verify from simulations since one needs to study very large system sizes to reach the correct asymptotic limit. The reason for this can be roughly seen

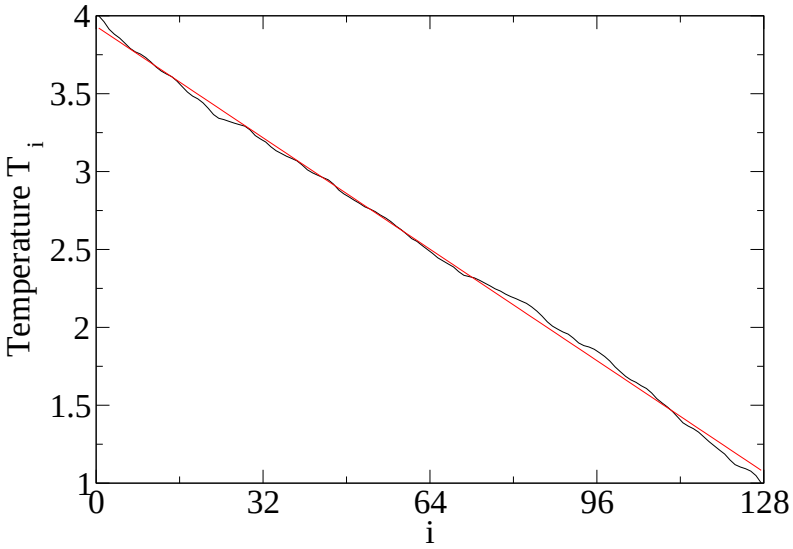

Figure 3.11: Plot of temperature profile ($T_i = \langle p_i^2/m_i \rangle$) for the unpinned case (with mass disorder $\Delta = 0.8$) with fixed BCs for $N = 128, \lambda = 5, T_L = 4, T_R = 1$. The expected linear profile is also shown. The data was obtained from exact numerical computation.

as follows. In the ordered case the conductivity $\kappa \sim 1/\lambda$ and this can be understood in terms of an effective mean free path $\ell \sim 1/\lambda$ for the ballistic phonons because of scattering from the stochastic process. Hence we can expect that, to see diffusive behavior for the low frequency ballistic modes, important in the disordered case, requires one to study sizes $N \gtrsim \ell$ or $N \gtrsim 1/\lambda$. Finally we observe from Fig. 3.10 that at small λ, the conductivity appears to be diverging as $1/\lambda^{1/2}$. In the absence of noise the localization length $\ell_L \sim 1/\omega^2$, hence it is expected that all modes with $\ell_L < \ell$ or $\omega > \lambda^{1/2}$ stay localized. The low frequency modes $0 < \omega < \lambda^{1/2}$ become diffusive with mean free paths $\sim 1/\lambda$ thus resulting in a conductivity $\kappa \sim \lambda^{1/2}(1/\lambda) \sim 1/\lambda^{1/2}$, which explains the observed behavior.

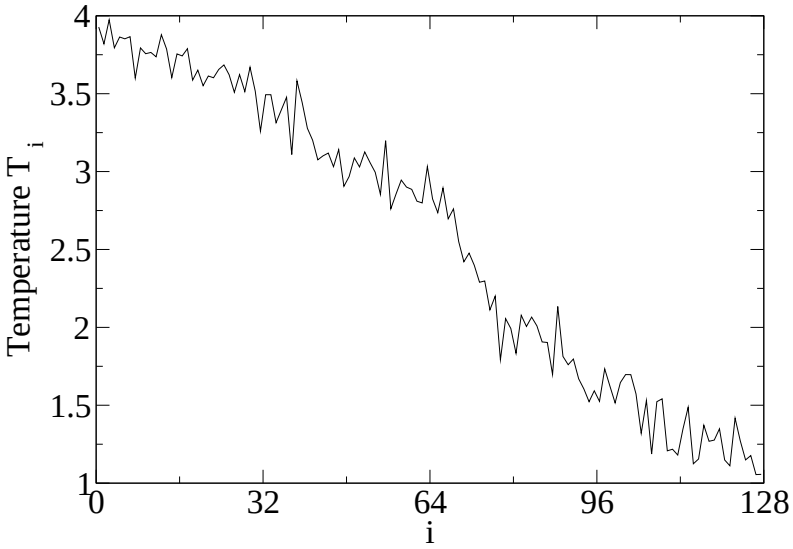

Figure 3.12: Same parameters as Fig. 3.11 except the velocity flip $\lambda \to 0$. The data shown is from an exact numerical computation with $\lambda = 10^{-9}$. We have verified that this is close to the temperature profile for $\lambda = 10^{-7}$ and expect that it is converging to the $\lambda = 0$ value.

3.7 Higher Order Correlations

The NESS of self-consistent reservoirs model is exactly Gaussian but this is not so for our noisy model. Instead it will be in general a superposition of Gaussians. Computer simulations however indicate that the single particle distributions are very close to a single Gaussian while the joint distribution of x_l and p_l or of p_l and p_j , $j \neq l$, are essentially uncorrelated. In addition, the set of equations for the four variable correlation functions was derived and for small values of n, they were solved numerically. The exact values obtained from these numerics were found to be in close match with the simulation results. For n=4, and $T_L = 4, T_R = 1$, the results from the numerical solution are shown in Table 3.1 corresponding to 3 different values of λ. It was also observed that these normalized forms of correlations (that go to zero when the temperatures of the two reservoirs are equal or when there is no velocity flipping) have

Table 3.1: Values of Correlation Functions for n=4 ($T_L = 4, T_R = 1$)

Correlation	$\lambda = 0.1$	$\lambda = 2$	$\lambda = 10$
$\frac{<p_1^4>-3<p_1^2>^2}{<p_1^2>^2}$	0.006	0.014	$\sim 10^{-4}$
$\frac{<p_2^4>-3<p_2^2>^2}{<p_2^2>^2}$	0.054	0.058	0.049
$\frac{<p_3^4>-3<p_3^2>^2}{<p_3^2>^2}$	0.061	0.110	0.098
$\frac{<p_4^4>-3<p_4^2>^2}{<p_4^2>^2}$	0.038	0.018	0.002
$\frac{<p_1^2q_1^2>-<q_1^2><p_1^2>}{<q_1^2><p_1^2>}$	0.002	0.004	$\sim 10^{-5}$
$\frac{<p_2^2q_2^2>-<q_2^2><p_2^2>}{<q_2^2><p_2^2>}$	0.011	0.014	0.013
$\frac{<p_3^2q_3^2>-<q_3^2><p_3^2>}{<q_3^2><p_3^2>}$	0.012	0.025	0.023
$\frac{<p_4^2q_4^2>-<q_4^2><p_4^2>}{<q_4^2><p_4^2>}$	0.012	0.034	$\sim 10^{-4}$

a limit when either the difference in temperature ($T_L - T_R$) or strength of stochastic noise (λ) goes to infinity. When we let $\lambda \to \infty$, we observed that the correlations involving p1 and p4 went to zero.

We are currently investigating the $O(N)$ corrections to the pair correlations in the noisy NESS . These are known to behave like $1/N$ for certain diffusive lattice systems and to contribute terms of $O(N)$ beyond those obtained from the local equilibrium to the variance of the particle number in the NESS. Results of this kind are also known partially for the continuum case with a different kind of noise, i.e instead of velocity reversals pairs of nearest neighbor particles diffuse on the circle $p_i^2 + p_{i+1}^2 = C$.

3.8 Fluctuations

We can analyze the macroscopic fluctuations in the energy profile of the ordered mass chain using the theory of large deviations. We first establish the macroscopic equations using the hydrodynamical scaling limit.

3.8.1 Hydrodynamical Equations

The unpinned chain

When $k_0 = 0$ the *bulk* dynamics conserves two quantities. The first one is the energy H. The second one is the deformation, $\sum_j r_j$ of the lattice, with $r_j = q_{j+1} - q_j$, $j = 0, 1, \ldots, N$. This second conservation law has to be taken into account in the hydrodynamic analysis.

Setting the masses to unity, the energy at a site $j \in \{1, \ldots, N\}$ is now given by

$$\mathcal{E}_j = \frac{p_j^2}{2} + k_1 \frac{r_j^2}{4} + k_1 \frac{r_{j-1}^2}{4} \tag{3.22}$$

and $\mathcal{E}_0 = \frac{1}{4} k_1 r_0^2$, $\mathcal{E}_{N+1} = \frac{1}{4} k_1 r_N^2$. To establish the hydrodynamic limits corresponding to the two conservation laws, we look at the process with time scaled by N^2 and space scaled by N, i.e., in the diffusive scale [38]. Assume that initially the process is started with a Gibbs local equilibrium measure $\hat{P}$ associated with a macroscopic deformation profile $u_0(q)$ and a macroscopic energy profile $\varepsilon_0(q)$:

$$\hat{P} = \frac{1}{Z} \prod_{j=0}^{N+1} \exp\left\{-\beta_0(j/N)(\mathcal{E}_x - \tau_0(j/N) r_j)\right\}, \tag{3.23}$$

where $T_0 = \beta_0^{-1}$ and τ_0 are the temperature and tension profiles corresponding to the given energy and deformation profiles assumed to be continuous. Then we have for any macroscopic point $q \in [0, 1]$

$$\lim_{N\to\infty} \langle r_{[Nq]}(0) \rangle = u_0(q), \quad \lim_{N\to\infty} \langle \mathcal{E}_{[Nq]}(0) \rangle = \varepsilon_0(q), \tag{3.24}$$

where $[y]$ is the integer part of y and the averages are w.r.t. $\hat{P}$.

The question then is: what happens at any later (macroscopic) time t? We define

$$\lim_{N\to\infty} \langle r_{[Nq]}(N^2 t)\rangle = u(q,t), \quad \lim_{N\to\infty} \langle \mathcal{E}_{[Nq]}(N^2 t)\rangle = \varepsilon(q,t)\,, \tag{3.25}$$

and we show in Appendix A that u, ε are solutions of the following macroscopic diffusion equation

$$\begin{cases} \partial_t u = \frac{k_1}{2\lambda}\,\partial_q^2\, u \\ \partial_t \varepsilon = \frac{k_1}{4\lambda}\,\partial_q^2\,(\varepsilon + k_1 u^2/2) \end{cases} \tag{3.26}$$

with the initial conditions $u(q,0) = u_0(q)$, $\varepsilon(q,0) = \varepsilon_0(q)$. Eq (3.26) is to be solved subject to the boundary conditions

$$\begin{aligned} &\partial_q u\,(0,t) = \partial_q u\,(1,t) = 0, \\ &\left(\varepsilon - \frac{u^2}{2}\right)(0,t) = T_L, \quad \left(\varepsilon - \frac{u^2}{2}\right)(1,t) = T_R\,. \end{aligned} \tag{3.27}$$

The proof for the boundary condition on $\partial_q u$ is given in the Appendix B.
Taking the limit $t \to \infty$ in these equations we obtain the typical macroscopic profiles of the system in the NESS, i.e., a flat deformation profile $u = 0$ and a linear profile $\bar{T}$ interpolating between T_L and T_R,

$$\varepsilon(q) = \bar{T}(q) = T_L + (T_R - T_L)q\,, \tag{3.28}$$

for the energy profile.

The pinned chain

Assume that the system is initially distributed according to a Gibbs local equilibrium measure associated to the energy profile $\varepsilon_0(q)$, $q \in [0,1]$, and define $\varepsilon(q,t)$ as the

evolved profile in the diffusive scale, i.e.,

$$\varepsilon(q,t) = \lim_{N\to\infty} \langle \mathcal{E}_{[Nq]}(tN^2) \rangle \,.$$

Then ε is the solution of the following heat equation (as shown in the Appendix A.2)

$$\begin{cases} \partial_t \varepsilon = \partial_q(\kappa \partial_q \varepsilon)\,, \\ \varepsilon(q,0) = \varepsilon_0(q)\,, \\ \varepsilon(0,t) = T_L,\ \varepsilon(1,t) = T_R\,. \end{cases} \tag{3.29}$$

When t goes to infinity $\varepsilon(q,t)$ converges to the linear profile $\bar{T}(q)$ (given in (3.28)) both for the velocity-flip and the self-consistent model. We note finally that, since the self-consistent model does not conserve energy in the bulk, we do not expect any autonomous macroscopic equations in that model.

3.8.2 Energy Fluctuations

The pinned chain

Our goal is to estimate the probability that in the stationary state the empirical energy profile, $\theta^N(q)$, defined by looking at the microscopic energy $\mathcal{E}_x$, for x equal to the integer part of Nq, is close to a prescribed macroscopic energy profile $e(q)$ different from $\bar{T}(q)$, i.e., we want to find the large deviation function (LDF) for the NESS.

At equilibrium $T_L = T_R = T = \beta^{-1}$ the stationary state coincides with the usual Gibbs equilibrium measure $P_T^{N,\mathrm{eq}}$ and by the usual large deviations theory (see e.g. [39]) we have that for any given macroscopic energy profile $e(\cdot)$

$$P_T^{N,\mathrm{eq}}\left(\theta^N(q) \sim e(q)\right) \sim e^{-NV_{\mathrm{eq}}(e)} \tag{3.30}$$

where the large deviation function (LDF)

$$V_{\text{eq}}(e) = \int_0^1 \left[\frac{e(q)}{T} - 1 - \log\left(\frac{e(q)}{T} \right) \right] dq$$

coincides with the difference between the free energy of the system in local thermal equilibrium (LTE) and the true equilibrium free energy with $e(q) = T$.
Out of equilibrium ($T_L \neq T_R$) there is also a large deviation principle [40]

$$P^N \left(\theta^N(\cdot) \sim e(\cdot) \right) \sim e^{-NV(e)}$$

but the explicit form of V is in general unknown. What is true however, is that V depends only on two macroscopic quantities: the heat conductivity and the mobility [40].
By the Einstein relation the mobility $\chi(T)$ is equal to $\chi(T) = \kappa(T)\sigma(T)$ where $\sigma(T)$ is the static compressibility defined by the equilibrium correlation

$$\sigma(T) = \sum_{j \in \mathbb{Z}} \langle (\mathcal{E}_0 - T)(\mathcal{E}_j - T) \rangle^{(\text{eq},T)}. \tag{3.31}$$

A simple computation shows that for our system $\sigma(T) = T^2$ and Theorem 6.5 of [40] applies. It follows that $V(\cdot)$ is given by

$$V(e) = \int_0^1 dq \left[\frac{e(q)}{F(q)} - 1 - \log\left(\frac{e(q)}{F(q)} \right) - \log\left(\frac{F'(q)}{T_R - T_L} \right) \right], \tag{3.32}$$

where F is the unique increasing solution of

$$\begin{cases} \dfrac{\partial_q^2 F}{(\partial_q F)^2} = \dfrac{F-e}{F^2}\,, \\ F(0) = T_L,\ F(1) = T_R\,. \end{cases} \tag{3.33}$$

Surprisingly, the function V is independent of the pinning value k_0 and of the intensity of the noise λ. In fact, it coincides with the LDF of the Kipnis-Marchioro-Presutti (KMP) model considered in [41]. In that model the dynamics are entirely stochastic. It is now easy to derive the Gaussian fluctuations of the empirical energy. We consider a small perturbation, $e = \bar{T} + \delta h$, of the stationary profile $\bar{e}$. The functional V has a minimum at $\bar{T}$ so that

$$V(e) = V(\bar{T}) + \frac{1}{2}\delta^2 \langle h, C^{-1} h\rangle + o(\delta^2)$$

The operator C is the covariance for the Gaussian fluctuations of the empirical energy under the invariant measure $\mu^N_{\mathrm{s,v}}$. The computations are the same as in [41] and we get

$$C = \bar{T}^2 \mathbf{1} + (T_R - T_L)^2(-\Delta_0)^{-1} \tag{3.34}$$

where Δ_0 denotes the Laplacian with Dirichlet boundary conditions on $[0,1]$.

Unpinned Chain

For the unpinned case, we are not able to obtain the expression of the LDF of the two conserved quantities nor for the energy alone. We conjecture that the LDF for the energy is the same for the pinned and unpinned case. Moreover, we are able (under suitable assumptions) to show that, in the unpinned case, (3.34) is still valid [51].

N	T_ℓ, T_r	λ	$\tilde{s}_N$	Error $\lvert s_\infty - \tilde{s}_N \rvert$	$s_\infty^{\text{loc.eq.}}$	s_∞
100	8,1	0.1	1.40	0.01		
200	8,1	0.1	1.39	0.01	1.20	1.40
400	8,1	0.1	1.42	0.02		

Table 3.2: Total energy variation in the unpinned model ($k_0 = 0$).

3.8.3 Numerical simulations

We performed numerical simulations for the velocity-flip model as described earlier Sec. 3.6 to calculate the fluctuations in the energy. We ran the program for a considerably longer time than before to obtain reliable data.

The total energy H is given by (3.1), and our goal is to estimate numerically its total fluctuations, by measuring the observable

$$s_N = N \frac{\langle H^2 \rangle - \langle H \rangle^2}{\langle H \rangle^2}.$$

Using equation (3.34) the measured fluctuations in the total energy should be given by

$$s_\infty = \lim_{N \to \infty} s_N = s_\infty^{\text{loc.eq.}} + c_\infty \,,$$

where $s_\infty^{\text{loc.eq.}} = \int_0^1 \bar{T}^2(q)dq / \Big[\int_0^1 \bar{T}(q)dq\Big]^2$ is the value we would obtain by a local equilibrium approximation, and $c_\infty = \frac{1}{12}(T_r - T_\ell)^2 / \Big[\int_0^1 \bar{T}(q)dq\Big]^2$ is the correction due to the long-range correlations. The prefactor $\frac{1}{12}$ is obtained by integrating over $((-\Delta_0)^{-1}1)(q) = q(1-q)/2$. Computing the remaining explicit integrals yields then

$$s_\infty = \frac{4T_\ell T_r + \frac{5}{3}(T_r - T_\ell)^2}{(T_\ell + T_r)^2}.$$

To get good statistics, several realizations of the initial data were considered. The results from numerical simulations for the variation in total energy, denoted by $\tilde{s}_N$, are collected in Tables 3.2 and 3.3. These results are compared with the theoretical

N	T_ℓ, T_r	k_0	λ	$\tilde{s}_N$	Error $\lvert s_\infty - \tilde{s}_N \rvert$	$s_\infty^{\text{loc.eq.}}$	s_∞
200	8,1	0.25	0.1	1.38	0.01		
200	8,1	0.5	0.1	1.39	0.01		
200	8,1	0.25	1.0	1.39	0.02	1.20	1.40
400	8,1	0.25	0.1	1.39	0.01		
800	8,1	0.25	0.1	1.46	0.05		
200	5,1	0.25	0.1	1.30	0.01	1.15	1.30

Table 3.3: Total energy variation in the pinned model ($k_0 > 0$).

estimate, s_∞, and with $s_\infty^{\text{loc.eq.}}$. We see that there is a very close match between the predicted s_∞ and the measured values.

3.9 Discussion

We have shown here that the stationary one-body and pair correlations in the velocity flip model are the same (after setting $\gamma_l' = 2\lambda m_l$) as in the harmonic chain with self-consistent reservoirs. We have used this to caclulate the conductivity of the ordered mass chain as $N \to \infty$. This result was also arrived at using the Green-Kubo formula. In the case of disordered masses, we used the Green-Kubo formula to establish bounds for the conductivity. To understand further, we numerically investigated the system and explored the dependence of the thermal conductivity κ on the velocity flip rate λ (and others such as mass disorder Δ and the pinning strength k_0). For $\lambda \to 0$ our results suggest $\kappa \sim \lambda$ for the pinned system. When the chain was unpinned, the exact numerics and numerical simulations pointed to the fact that the conductivity κ does not depend on the boundary conditions (as we should expect from a real system where conductivity is a bulk property). Our results suggest that $\kappa \sim \lambda^{-1/2}$ for the unpinned system although establishing these results conclusively requires further work. We have also shown that the steady state of the system is not exactly Gaussian as it is for the case of the self-consistent model.

Furthermore, we studied the flucutations in the total energy of the system. To do this,

we obtained the hydrodynamical equations for our system, applied the theory of large deviations of non-equilibrium systems to calculate the fluctuations in the macroscopic profile of the energy. We obtained a good match between this theoretical result and the data from numerical simulations of the system.

Chapter 4

1-D Chains with Anharmonicity and Noise

4.1 Introduction

The preceding two chapters have dealt with systems where the Hamiltonian consists of only nearest neighbor harmonic interactions. In real materials, we most often observe a more complex interaction which results in the net force on a particle having nonlinear components. It is partly to account for these nonlinearities that we introduce stochastic dynamics which makes the system more tractable analytically. In this chapter, we shall consider systems with both nonlinearity and anharmonicity and explore their combined effects.

While a large class of harmonic systems with noise have been solved exactly, this is not the case for anharmonic systems where there are just a few exact results [45][46], and most of our knowledge about the behavior and properties comes from numerical simulations. In fact, even a phenomenological understanding of such systems is not very deep. Such 1d systems are not only of theoretical but also of practical interest

[42], [43].

Here, we present the details of investigations of a one-dimensional chain of particles with anharmonic interactions through numerical simulations. We consider both ordered-mass and disordered-mass chains, with and without stochastic bulk noise, and examine the behavior of the heat current and its dependence on various parameters of the model.

In the case of ordered mass systems with inter-particle harmonic coupling and non-linear pinning, numerical results suggest that they exhibit normal conductivity[47, 48]. However, the effects of non-linearity which changes the conductivity from being infinite to a finite value is non-perturbative, and we do not understand the dependence of the conductivity on the anharmonicity[44].

Our idea has been to approach this very challenging problem in a more indirect manner. In addition to non-linear pinning term, we include random dynamics in the bulk of the system. Our analysis of harmonic systems with bulk stochastic dynamics in Chapter 3 indicated that we obtain normal conductivity and for ordered systems, we had derived an exact expression for heat current(see 3.3). We may then expect (hope) that, for systems with both anharmonicity and stochastic bulk dynamics, a perturbative approach will be valid in the anharmonic interaction term. We also want to study what happens as we the strength of the bulk noise goes to zero, which corresponds to anharmonic systems with Hamiltonian bulk dynamics. Introduction of random dynamics also improves the convergence of simulation. The stochastic dynamics we have considered in this simulation is a random velocity flipping at every site.

4.2 Model

We write the Hamiltonian of the chain as before except that we introduce an additional term for quartic pinning:

$$H = \frac{1}{2}\sum_{i=1}^{i=N} p_i^2/2m_i + \frac{1}{2}\sum_{i=1}^{N+1} k_1(q_i - q_{i-1})^2 + \frac{1}{2}\sum_{i=1}^{N} k_0 q_i^2 + \frac{1}{4}\sum_{i=1}^{N} k_3 q_i^4 \qquad (4.1)$$

where, as earlier, k_1 and k_0 are the harmonic nearest neighbor interaction and pinning potential coefficients respectively, and k_3 is the anharmonic pinning coefficient.
Once again, the equations of motion of the end particles interacting with the Langevin heat baths at temperatures T_L and T_R are given by:

$$\begin{aligned} m_i\ddot{q}_i &= -k_1(2q_i - q_{i-1}\delta_{i,N} - q_{i+1}\delta_{i,1}) - k_0 q_i - k_3 q_i^3 \\ &+ \delta_{i,1}[-\gamma_L\dot{q}_1 + (2\gamma_L T_L)^{1/2}\eta_L] + \delta_{i,N}[-\gamma\dot{q}_N + (2\gamma T_R)^{1/2}\eta_R] \ , \end{aligned} \qquad (4.2)$$

where γ is the strength of the coupling to the reservoirs

The stochastic dynamics is generated by velocity reversals at every site, $v_i \to -v_i$ indepdendently at a rate λ.
The numerical simulations are carried out in a manner identical to the previous systems we have considered.

For harmonic systems with or without stochastic velocity flips, the heat current depends linearly on the difference in temperature at the ends while for non-linear chains, this will generally not be true. In other words, the heat conductivity will in general depend on the temperature. To obtain the conductivity directly from the simulations requires that the difference in the reservoir temperatures be small compared to their

average, i.e, $\frac{T_L-T_R}{T_L+T_R} << 1$. Yet, in many of our simulations, the reservoir temperatures are $T_L = 2$ and $T_R = 1$, which gives $\frac{T_L-T_R}{T_L+T_R} = \frac{1}{3}$, a fairly large number. This is because, as we shall describe in more detail below, obtaining a consistent and reliable value for the heat current becomes more difficult as the temperature difference is made smaller.

4.3 Results

Case (a) : Ordered Chains

We ran several sets of simulations for equal mass chains with bulk anharmonic pinning, harmonic nearest neighbor interactions and stochastic noise (velocity flip). Our aim was to consider how the heat current depends on the combination of non-linearity and stochasticity in the system. For a given length of the chain N, with k_0 and k_1 kept fixed, we varied k_3 and λ. The heat current $j_i = -\frac{1}{2}\langle(v_{i+1} + v_i)(q_{i+1} - q_i)\rangle$, where $\langle.\rangle$ refers to ensemble average, is calculated for every pair of nearest neighbors in the chain, and ultimately, we take the average over these for $i = 2, 3, \cdots N-1$ to determine the mean current through the chain. We also calculate the difference σ_j between the maximum and the minimum value of j_i. It was noticed that, for most choices of the parameters k_3 and λ, σ_j was less than 5% of the average current, and this bound on was found to be true over several runs of the simulations. As for system parameters where this was the case, we have taken σ_j to be the overall error margin for the current. The effective conductivity for a system of size N, κ_N, is defined as $J(N)N/(T_L - T_R)$ and the error in conductivity was obtained by error propagation scheme: error in κ_N is given by $\sigma_j N/(T_L - T_R)$.

In other cases where σ_j was greater than 5% of the mean current, a set of four

separate simulations were carried out and the conductivity for each was obtained, κ^l, $l = 1, \cdots 4$. The average conductivity $\bar{\kappa}$ was determined by taking the arithmetic mean and error in the mean conductivity taken to be:

$$\frac{\sqrt{\sum_{j=1}^{4} \kappa^{j2} - \bar{\kappa}^2}}{4}.$$

The conductivities obtained from the simulations are shown in Table 4.1, for $N =$ 200, 400 and 800. The error in the last decimal place of the data value appears next to the entry (in brackets).

For completeness, we have also included the conductivity in the case of pure noise ($k_3 = 0$) and pure anharmonicity ($\lambda = 0$). The latter system can be solved by exact numerics by solving for the correlation matrix (as discussed in the previous chapter (see Sec. 3.6). We could perform this technique only for $N < 475$ and in these instances, the error is very small -less than 0.001% - and hence we do not provide any the error estimate.

There are several immediate observations we can make looking at the table. The first is that conductivity $\kappa_N = JN/(T_L - T_R)$ does not saturate as we increase N from N=200 to N=800, for $\lambda \leq 0.01$ This feature is seen in the Fig. 4.1 as well. We also note that $\kappa_N(\lambda, k_3)$, in all but one instance, decreases monotonically with increase in either stochastic strength or anharmonicity. This can be seen in Fig. 4.2 and Fig. 4.3 for $N = 800$. It must be remembered that the conductivity has not saturated for every data point on these plots.

We were having numerical accuracy problems for simulations with $N \geq 1600$, and so we do not have a complete picture of the behavior of the system, especially when $\lambda \lesssim 0.01$, the region of parameter space where the convergence in conductivity occurs beyond $N = 800$.

Perturbative Expansion

$N = 200$		Velocity Flip Rate λ					
		0	0.0001	0.001	0.01	0.1	1.0
k_3	0	27.0	26.0	20.8	7.0	0.94	0.1
	0.0001	26.5(1)	26.66(4)	20.8(1)	6.94(4)	0.98(2)	0.106(6)
	0.001	26.9(1)	26.0	20.7(1)	6.90(2)	0.96(2)	0.092(8)
	0.01	26.08(8)	25.58(6)	20.6(1)	6.90(4)	0.94(2)	0.096(2)
	0.1	18.3(1)	18.00(4)	15.22(8)	7.96(2)	0.84(2)	0.088(2)
	1.0	2.02(2)	1.98(2)	2.02(4)	1.54(2)	0.52(2)	0.068(2)

$N = 400$		Velocity Flip Rate λ					
		0	0.0001	0.001	0.01	0.1	1.0
k_3	0	53.6	50.4	34.0	8.0	0.88	0.08
	0.0001	53.8(2)	50.1(2)	34.4	8.04(8)	0.8(1)	0.092(4)
	0.001	53.3(2)	50.1(2)	33.7(2)	8.1(1)	0.88(8)	0.084(4)
	0.01	52.4(3)	49.8(3)	33.5(2)	8.0(1)	0.88(8)	0.088(4)
	0.1	28.7(1)	27.9(2)	21.9(2)	6.88(8)	0.80(8)	0.084(4)
	1.0	2.1(2)	2.2(1)	2.1(1)	1.64(8)	0.52(8)	0.065(2)

$N = 800$		Velocity Flip Rate λ					
		0	0.0001	0.001	0.01	0.1	1.0
k_3	0	0.106.7(1)	96.0(4)	49.8(2)	8.7(1)	0.9(1)	0.10(1)
	0.0001	107.8(3)	96.5(4)	50.5(1)	8.8(8)	0.96(8)	0.09(2)
	0.001	106.4(3)	95.8(5)	49.4(4)	8.8(3)	1.0(1)	0.08(2)
	0.01	104.1(1)	93.6(5)	49.1(1)	8.5(2)	1.0(1)	0.09(2)
	0.1	41.2(2)	39.1(3)	27.6(2)	7.1(2)	0.9(1)	0.09(2)
	1.0	2.22(2)	2.2(2)	2.2(2)	1.6(2)	0.5(2)	0.07(2)

Table 4.1: Variation of conductivity for an ordered chain with velocity flip rate λ and quartic pinning coefficient k_3

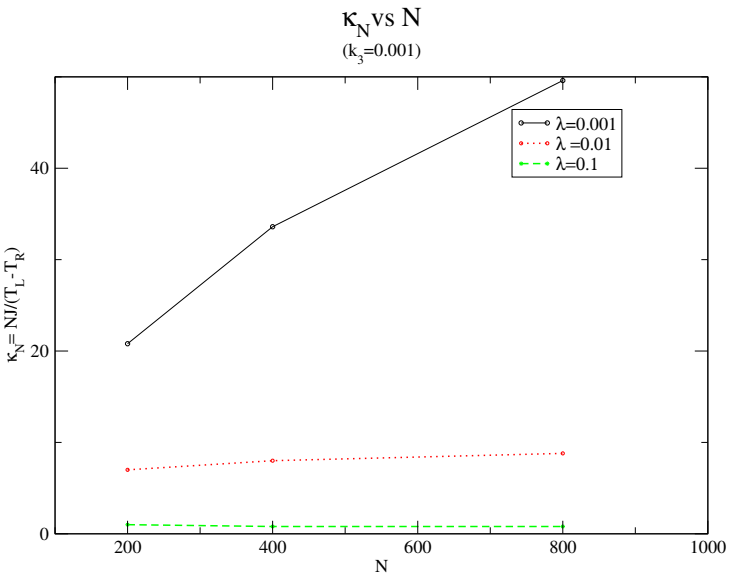

Figure 4.1: Plot of conductivity $\kappa_N = JN/(T_L - T_R)$ as a function of N, for different values of λ (k_3 is fixed at 0.0001). Observe that the curves become flat, i.e., approach the infinite N limit, only for $\lambda \gtrsim 0.01$

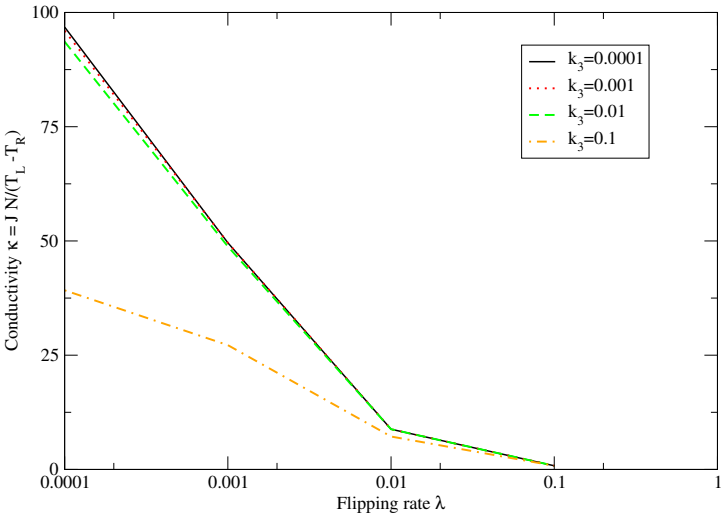

Figure 4.2: Plot of conductivity vs. stochastic strength for various values of anharmonic pinning coefficient k_3 ($N = 800$).

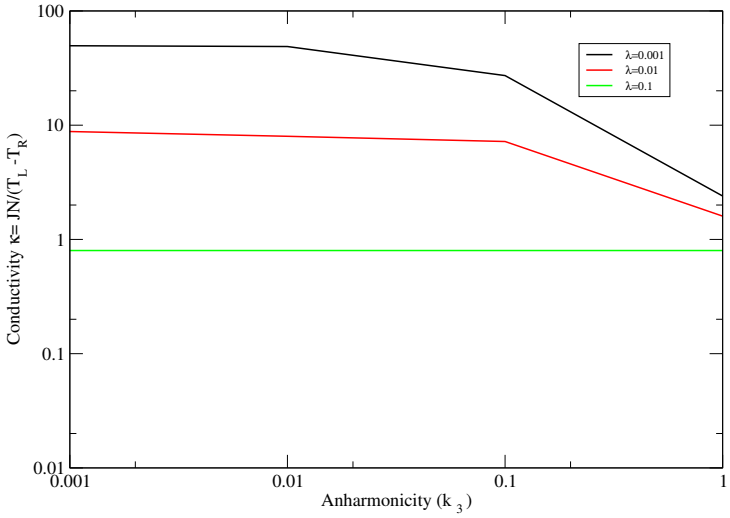

Figure 4.3: Plot of conductivity vs. anharmonic strength for various values of the stochastic strength λ ($N = 800$). Notice how the curves are nearly flat in the region $k_3 \lesssim 0.1$.

The conductivity that is conjectured to arise when we add a small anharmonic term to a pinned harmonic ordered chain is considered to be non-perturbative in origin. The pinned harmonic ordered chain with random velocity flips, however, has been shown to have normal conductivity. Hence, an addition of non-linear pinning term to such a system, would produce a change in conductivity that can be expected to be perturbative. In this spirit, the first two terms of the perturbation expansion in the anharmonic coefficient for the infinite-system conductivity has been derived using the Green-Kubo formula (keeping λ fixed) ([49]).

$$\kappa_T(\lambda, k_3) = \kappa(\lambda, 0) - 3\frac{k_3 T}{\lambda}\frac{(\sqrt{4+k_0} - \sqrt{k_0})^2}{2k_0(4+k_0)} + \text{...higher order terms...} \qquad (4.3)$$

where

$$\kappa(\lambda, 0) = \frac{k_1^2}{2\lambda m(2k_1 + k_0 + \sqrt{k_0(4k_1+k_0)})}$$

Note that the first order correction to the heat conductivity is linear in the temperature T.

The data discussed so far is unsuitable for testing this first order approximation formula because, as we saw in Fig. 4.3 the change of conductivity with $k_3 \lesssim 0.1$ is too small (and of the same order as the error in the data). We may attribute this to the fact that k_0 is large in these simulations.

To obtain data that can be used to test the formula, we ran several more simulations. In these simulations, λ was fixed at 1.0, and N at 50 - large enough for the conductivity to be within 1% of what it is at the infinite N value.

It must be mentioned that there cannot be a convergent expansion in k_3 since a negative value of k_3 corresponds to an unbounded potential. To avoid this trap, we modified the potential to $V'(q) = \frac{1}{4}k_3 q^4 e^{-\alpha q^2}$, which, for $\alpha > 0$, is bounded regardless of the sign of k_3. By choosing $\alpha \ll 1$, we expect that, in numerical simulations, the systems will show identical behavior. Indeed, we were able to verify that this is the case for $\alpha = 0.02$, and for the parameters we have considered below in Table 4.2 (except for the last row).

We had to try several different values of k_0 bearing in mind that simulation must generate reliable and consistent heat current as well as produce a significant change in the current as we vary k_3. Finally, after a number of attempts, we settled on $k_0 = 0.6$

It is quite clear from the table above that the conductivities from the simulations and Eq. (4.3) do not agree. It is quite possible that the validity of the expansion holds only for $k_3 \ll 0.006$. However, given the numerical accuracy of our simulations it was impossible for us explore this regime.

Case (b) : Disordered Chains

Simulations with disordered masses are considerably more challenging than ordered

k_3	Conductivity	
	Simulation	First Order Approximation Formula
0	0.118(1)	0.1173
0.006	0.115(1)	0.1081
0.01	0.114(1)	0.1020
0.06*	0.110(1)	0.0255

Table 4.2: Comparison of the conductivities for a chain of length $N = 50$, between the value obtained from numerical simulations and that from the first order expansion in the anharminic coefficient k_3 as described in Eq.(4.3). In the simulations $T_L = 2$ and $T_R = 1$, and we have chosen T in Eq.(4.3) to be $\frac{T_L+T_R}{2}$. * For this case, the current from simulations with purely quartic potential came to 0.104(1).

chains. It is well known that disordered harmonic chains give rise to localization in some of the vibrational modes, and in the pinned case, all modes are localized leading to heat current that diminishes exponentially with the size of the system.

However, we have already learned from the previous chapter that when random velocity-flip dynamic is added to the system in bulk, the disordered harmonic chain exhibit normal conductivity (see 3.6). Moreover our results strongly indicated that Fourier's Law is valid for any non-zero strength of the noise.

At the same time, it has been shown using numerical simulations that normal conductivity is obtained for pinned disordered chains with non-linear interactions [34]. It still remains an open question if the transition from exponential decay to regular conductivity occurs at zero or at some finite value of the anharmonic strength. In other words, we do not know if any non-zero anharmonicity would destroy the localization produced by the disorder.

The approach here, as in the ordered system, is to combine the anharmonicity with noisy dynamics. It is reasonable to expect finite conductivity, $\kappa(\lambda, k_3)$, for arbitrary combination of random velocity flips of rate λ and anharmonicity k_3 (at infinite N). The interesting question would be to ask what happens when $\lambda \to 0$.

The data from our simulations is compiled in Table.(4.3), which shows the variation of the conductivity across λ and k_3. The harmonic pinning coefficient was kept fixed,

$k_0 = 0.25$, and the mass at each site comes from an independent identical distribution uniform in the interval [1-Δ, 1+Δ] with disorder strength $\Delta = 0.6$. The current for a given simulation realization was calculated using the same method as that of the ordered case. Since this a finite disordered system, the current will depend on the specific realization of the masses. The conductivity we have given in the table is calculated by taking the average of conductivities from the different realizations of the disorder. Shown along with the entries are also error bars which are calculated from the different realizations using the same method as described for ordered masses.

$N = 200$		λ			
		0.0001	0.001	0.01	0.1
k_3	0	0.49(3)	1.04(2)	1.7(1)	0.87(1)
	0.0001	0.42(6)	1.0(1)	1.4(2)	0.86(4)
	0.001	0.36(4)	1.0 (1)	1.8(2)	0.90(2)
	0.01	0.9(1)	0.76(4)	1.4 (2)	0.84(2)
	0.1	0.74(6)	0.70(2)	0.82(2)	0.56(2)

$N = 400$		λ			
		0.0001	0.001	0.01	0.1
k_3	0	0.25(1)	0.95(5)	1.88(5)	0.89(2)
	0.0001	0.28(4)	0.84(4)	2.0(1)	0.84(4)
	0.001	0.32(4)	0.80(4)	1.84(4)	0.88(4)
	0.01	0.60(4)	0.84(4)	1.56(4)	0.88(4)
	0.1	0.68(4)	0.84(4)	0.92(4)	0.64(4)

Table 4.3: Variation of conductivity for disordered chain with velocity flip rate λ and quartic pinning coefficient k_3. Errors indicated inside brackets refer to the final digit in the entry.

We plot the variation of conductivity with stochastic noise keeping the anharmonicity fixed in Fig. 4.4. We also plot the variation of conductivity with anharmonicity keeping the stochastic noise fixed in Fig. 4.5.

We remark on a few immediate observations about the graphs. The conductivity increases as we increase the stochastic noise when $\lambda \leq 1$, and beyond that point, it decreases. This behavior is similar to what we found in the disordered chain with only noise (cf. Chapter 3.6.1). Likewise, although it is not very apparent in the graph, Fig.

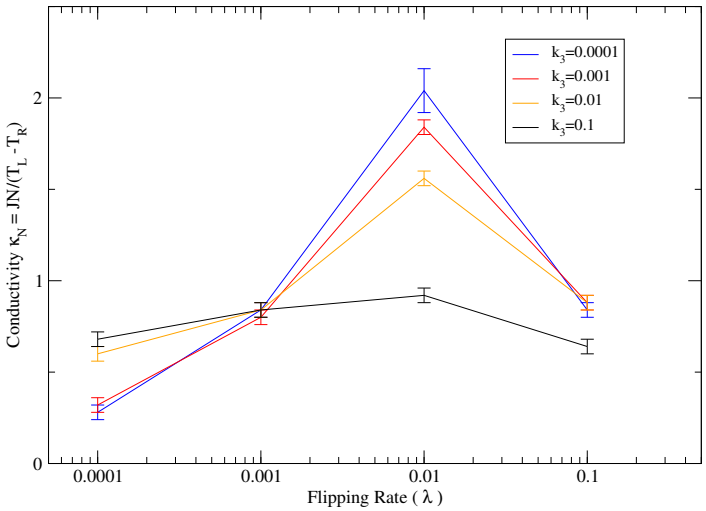

Figure 4.4: Plot of conductivity vs. stochastic strength for a various values of anharmonic pinning coefficient k_3 ($N = 400$).

4.5 shows the conductivity initially increasing with increase the anharmonic strength (for the curves where the fixed noise $\lambda < 0.01$). There is an eventual turnaround in the plot, beyond which, the conductivity decreases.

These observations indicate that both the stochastic noise and the anharmonicity have similar effects on the current characteristics of the system. Since we have already

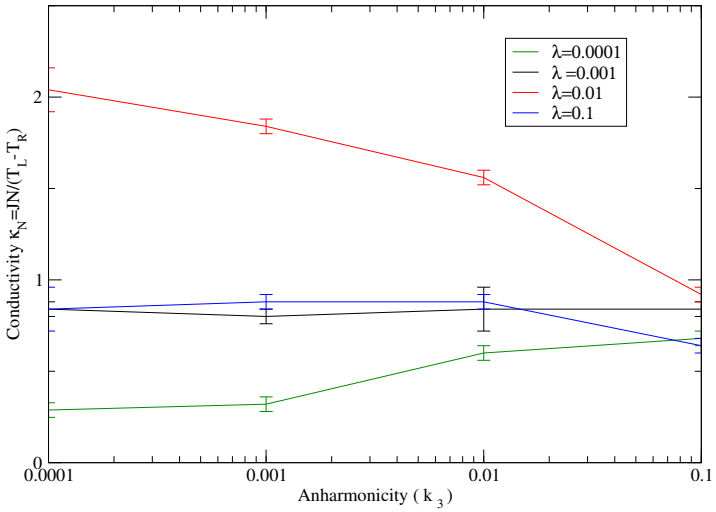

Figure 4.5: Plot of conductivity vs. anharmonic strength for various values of the stochastic strength λ ($N = 400$).

proven that any finite noise leads to normal transport in the disordered chain, we believe that the same would be true with addition of non-linear interactions. Yet, our data is very far from providing the necessary numerical evidence to convincingly establish this.

Chapter 5

Ordered Chain with Defect

5.1 Introduction

The class of systems we study here is the ordered, harmonic chains that have a single defect in the middle. The defect can be of the form of a particle with a mass different from the rest of the chain, a pinning coefficient at a site that is different from the others or a velocity flipping dynamics (of the nature we explored in Chapter 3) at a site on the chain. Finally defect can be created by introducing an anharmonic term added to the harmonic pinning at the defect site.

The interest in studying these models is to understand how the the temperature profile and the heat conductivity depend on the nature and the magnitude of the defect.

It is observed that the qualitative changes to the temperature profile and the heat flow of the system is similar for the various types of defects considered here. Whereas the temperature is a constant in the bulk for the uniform chain, the one dimensional system with a defect is characterized by two temperatures, one that is uniform to the left of the defect, and the other to the right of it. A sharp transition between these

two temperatures in the neighborhood of the defect is observed. Another common feature was that these two temperatures described above are independent, or vary very little, with the exact location of the defect.

Although most of our results are from exact numerics, a physical explanation is sought for the behavior based on the properties of one-dimensional harmonic chains. While some heuristic explanations are provided for the observed behavior, a systematic and thorough reasoning is still evading us.

5.2 Harmonic Chain with Mass Defect

The system we consider here is the one-dimensional chain with uniform masses everywhere expect at a single site in the bulk. The Hamiltonian for a chain of size N in this case is the given by Eq. (2.2) with the diagonal mass matrix $\mathbf{M}$ being unity everywhere expect at a single location u where it is m_0.

Since the procedure we have described earlier for obtaining the pair correlation in Chapter 2 (Eq.(2.7)) is for a generic configuration of masses, we solve the matrix equation numerically to obtain the temperature profile and the heat current.
The two plots (Fig. 5.1 and Fig. 5.2) show the temperature profile of the chain of size $N = 129$ for the two cases of the mass in the center, $m_0 \geq 1$ and $m_0 \leq 1$. It can be clearly seen that the temperatures in the bulk is split into two: one to the left of the defect, and the other to the right.

The variation of the temperature on the left segment of the chain with the mass of the defect m_0 is plotted in Fig. 5.3 and Fig. 5.4. The temperature is found to increases as the difference between the mass of the center site and the rest of the chain, $|m_0 - 1|$ increases. This behavior is expected since we can understand the defect as

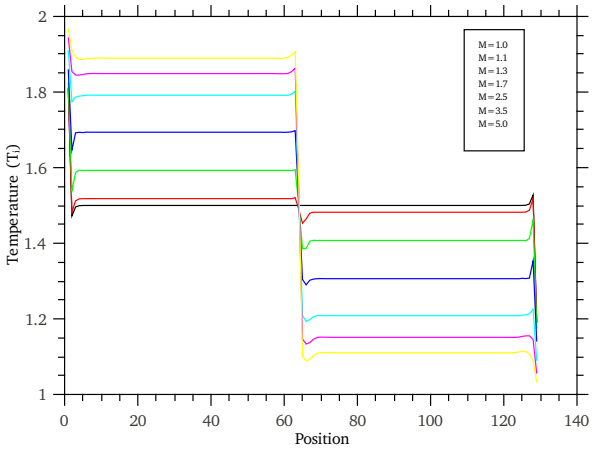

Figure 5.1: The various curves correspond to temperature profiles for a chain of length $N = 129$ with mass of the center particle m_0 equal to 1.0, 1.1,1.3,1.7,2.5,3.5 and 5 (all other masses are unity) respectively. The reservoir temperatures are $T_L = 2$ and $T_R = 1$. Observe the symmetry in the positive and negative deviance of temperature from the mean on the left and right hand side of the defect. Note also that the magnitude of the deviance increases with deviance of the defect mass m_0 from unity.

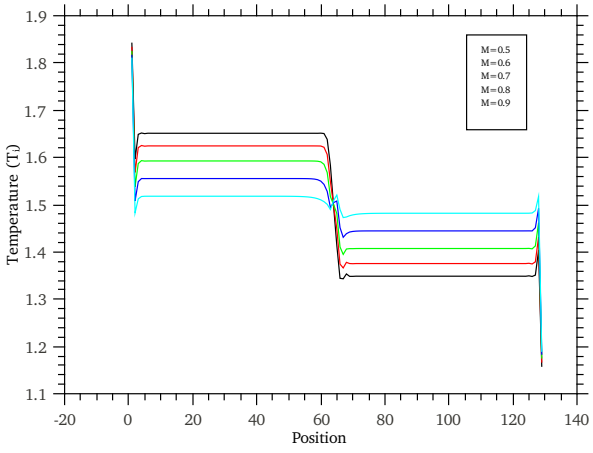

Figure 5.2: The various curves correspond to temperature profiles for a chain of length $N = 129$ with masses of the center particle equal to 0.5,0.6,0.7,0.8 and 0.9 (all other masses are unity). The reservoir temperatures are $T_L = 2$ and $T_R = 1$.Observe the symmetry in the positive and negative deviance of temperature from the mean on the left and right hand side of the defect. Note also that the magnitude of the deviance increases with deviance of the defect mass m_0 from unity.

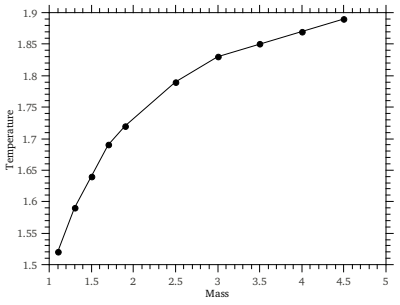

Figure 5.3: Temperature on the left segment of the profile plotted against the mass defect when $m_0 \geq 1$. Observe how the temperature is monotonically increasing from $\frac{T_L+T_R}{2} = 1.5$ as we increase m_0.

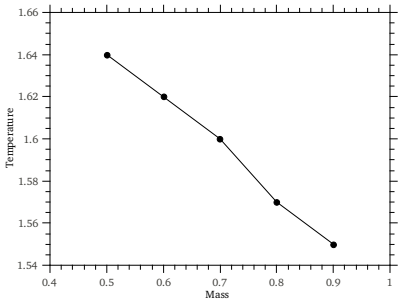

Figure 5.4: Temperature on the left segment of the profile plotted against the mass defect when $m_0 \leq 1$. Observe how the temperature is monotonically decreasing towards $\frac{T_L+T_R}{2}$ as we take m_0 closer to unity.

an impurity at which the phonons are scattered. In the process, the phonons that would otherwise exhibit ballistic transport is now partially reflected. However there is still unobstructed transport in the two segments, one between the left reservoir and the defect site, and the other between the defect site and the reservoir on the right, and these correspond to the regimes of uniform temperature. In the limit $m_0 \to \infty$, there will be no modes extended across the defect, and the steady state would split into two parts, namely, the left and right side of the defect, each of which would be at equilibrium with the left and right reservoirs respectively and thus have temperatures equal to T_L and T_R.

In Fig. 5.5 and Fig. 5.6, the heat current is observed to decrease as the deviation of mass of the defect from unity is increased. This dependence is again expected

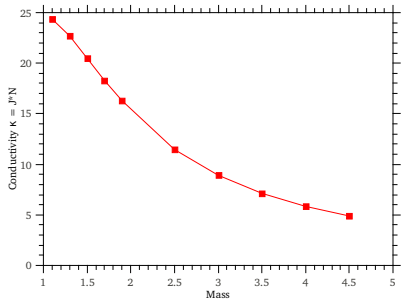

Figure 5.5: Conductivity of the chain plotted against the mass defect when $m_0 \geq 1$.

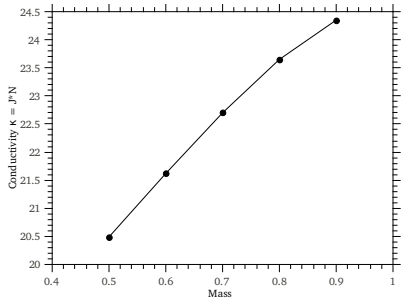

Figure 5.6: Conductivity of the chain plotted against the mass defect when $m_0 \leq 1$.

based on the reasoning that greater the difference of defect mass from the rest of the chain, greater is the scattering of the phonon modes at the defect site. As heat is carried across the chain by the phonons, this obstruction causes reduction in the heat current. In the limit $m_0 \to \infty$, we expect the current to go to 0.

5.3 Single Site Velocity Flip

We consider the ordered unpinned harmonic chain with a random velocity-flip dynamics at a single site. The behavior of the system is very similar to the case of the mass defect. In Fig.5.7, we plot the temperature profile for various flip rates. The uniform temperature regions on either side of the defect site can be immediately noted.

Fig. 5.8 shows the variation of the temperature of the left segment of a chain of length

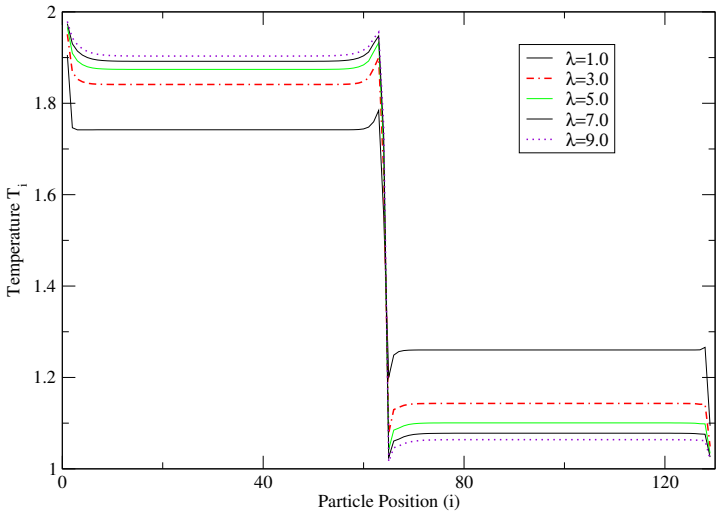

Figure 5.7: Temperature profile for an ordered harmonic chain of length $N = 129$ with random velocity flip dynamics at a single site ($u = 65$) with rate λ. The ends are connected to reservoirs maintained at temperatures $T_L = 2$ and $T_R = 1$.

$N = 129$ as a function of the rate of velocity flip at the center site. The explanation for this property can be ascribed to the scattering of the phonons at the defect, which results in partial reflection.

Fig. 5.9 plots the variation of the conductivity for the same chain against the velocity-flip rate λ. As in the earlier case of a mass defect, the conductivity decreases as we increase λ.

5.4 Anharmonic Pinning Potential

In this section, we consider the ordered pinned harmonic chain with a quartic pinning potential ($V_3(q) = 1/4k_3q^4$) to a single site at the center. The harmonic pinning potential k_0 is set to unity at all sites. Unlike the previous cases of defects created by a different mass or velocity flips, there is no analytic expression for the steady state characteristics. Hence, we run numerical simulations to determine the temperature profile and the current for this system.

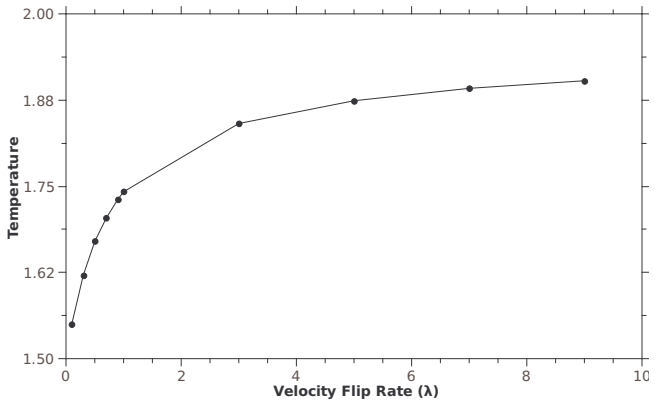

Figure 5.8: Temperature of the left segment of the chain vs rate of velocity-flip λ at the center site ($N = 129$). The ends are connected to reservoirs maintained at temperatures $T_L = 2$ and $T_R = 1$.

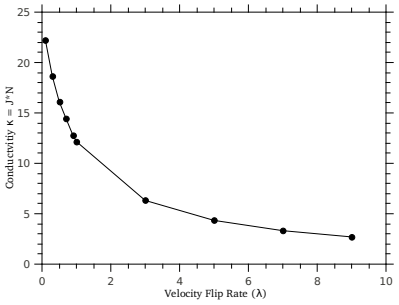

Figure 5.9: Variation of the conductivity with the rate of velocity-flip λ at the center site. The reservoir temperatures are maintained at $T_L = 2$ and $T_R = 1$.

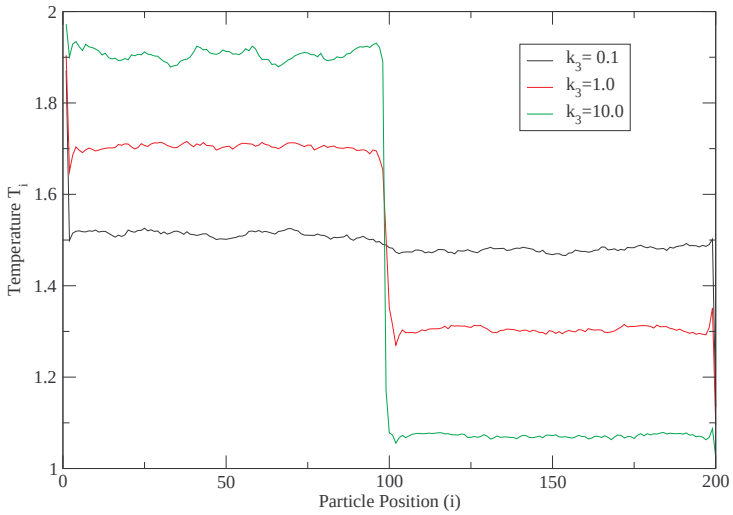

Figure 5.10: Temperature profile for a chain of length $N = 200$ for various values of quartic pinning potential at the center site. The ends are connected to reservoirs maintained at temperatures $T_L = 2$ and $T_R = 1$.

The simulations that we have considered here were performed using the same procedure as described in Chapter 4.2. In Fig. 5.10, we plot the temperature profile for three different values of the quartic pinning coefficient. Much like in the previous two cases, we get a profile that has a uniform temperature on either side of the site of anharmonic pinning. The waviness that is seen in the curve is due to the fact that the temperatures were calculated from numerical simulations.

The variation of the temperature in the left segment with the strength of quartic pinning at the center is plotted in Fig. 5.11.

Fig. 5.12 plots the variation of the conductivity as a function of the coefficient of the quartic potential. It can be immediately noted that the conductivity is mostly independent of the anharmonicity for $k_3 < 0.1$ and the subsequent decrease with

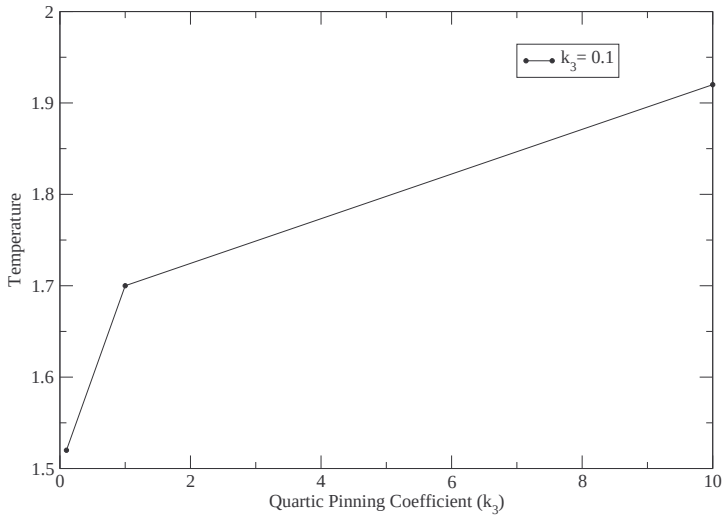

Figure 5.11: Temperature of the left segment of chain for various values of quartic pinning potential k_3 at the center site. The ends are connected to reservoirs maintained at temperatures $T_L = 2$ and $T_R = 1$.

increase in the strength of the pinning is more gradual than in the previous cases of defect created by mass and stochastic noise.

5.5 Conclusions

As stated earlier, several common features about the behavior of the system are evident from the graph. The temperature profiles for systems with the types of defect considered here splits into two flat sections, one between the left reservoir and the defect and the other, between the defect and the right reservoir (ignoring the boundary effects). This observation can be well explained by noting that these two segments can be regarded as ordered sub systems, and consequently, the phonons travel across their length without obstruction. At the defect site, there is scattering, and that accounts for the sharp temperature variations occurring in the immediate neighborhood of the defect.

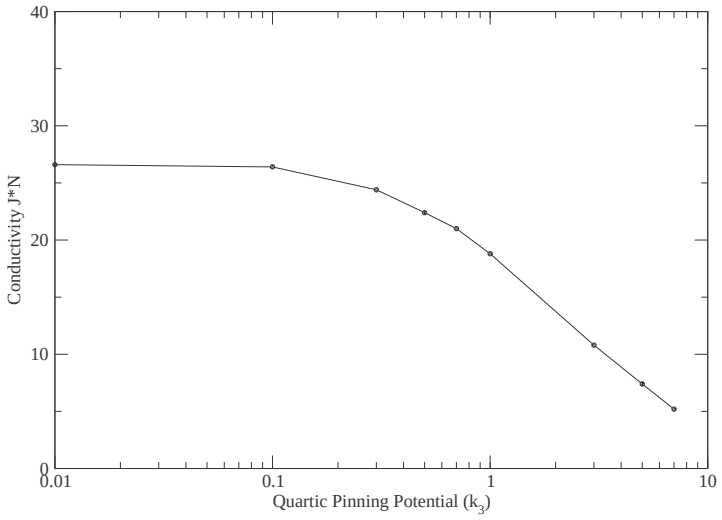

Figure 5.12: Variation of the conductivity of the chain of length $N = 200$ with the coefficient of the quartic pinning potential at the center site. The ends are connected to reservoirs maintained at temperatures $T_L = 2$ and $T_R = 1$.

Greater the magnitude of the defect, greater is the scattering and hence, more the sharp change in temperature between the two segments. This relationship between scattering and the defect also explains the decrease in current with the increase in the magnitude of the defect. The transmission amplitudes of the vibrational modes across the defect is lower when the magnitude of the defect is higher and this leads to decrease in corresponding decrease in average current.

The most prominent dissimilarity in the behavior of the system to the different types of defects considered here is the variation of current (conductivity) as the magnitude of defect is increased. This dependence for the anharmonic-pinning defect (Fig. 5.12) has two characteristics that sets it apart from the other cases (Fig. 5.5, 5.6, and

5.9): first, the current decreases more slowly with the defect strength and the second, it is concave downwards unlike the others. The first could possibly be the result of differences in scaling but we do not have a good explanation for the second. To understand it better, we will have to perform a quantitative analysis of the scattering at the defect.

Appendix A

Hydrodynamical Equations

We have to demonstrate that the variables $u(q), \varepsilon(q)$ defined in Eq.(3.25) satisfy the diffusion equations given in Eq.(3.26) for the unpinned chain and Eq.(3.29) for the pinned chain. Consider a generic equation that is defined on the interval $[0, 1]$ of the form:

$$\partial_t w = \partial_q(\sigma \partial_q y) \tag{A.1}$$

To prove that $w(q, t)$ and $y(x, t)$ satisfies the above equation, we need to show the following for all smooth functions $G : [0, 1] \to \mathbb{R}$ satisfying the boundary conditions $G(0) = G(1) = G'(0) = G'(1) = 0$.

$$\int_0^1 G(q)(w(q,t) - w(q,0))dq = \int_0^t \int_0^1 G(q)\frac{\partial}{\partial q}(\sigma(q)\frac{\partial}{\partial q}y(q,t))dqdt \tag{A.2}$$

Equivalently, given the boundary conditions on G, we need to show:

$$\int_0^1 G(q)(w(q,t) - w(q,0))dq = \int_0^t \int_0^1 G^{''}(q)\sigma(y)y(q,t)dqdt \tag{A.3}$$

A.1 Unpinned Chain

To prove the diffusion equation for energy given by Eq.(3.26), we will need to argue that it satisfies a relation of the form Eq.(A.3), with $w = \varepsilon$, $y = \varepsilon + u^2/2$ and $\sigma = 1/(4\lambda)$. We start from the microscopic variables for a chain of size N, and rewrite the heat current between sites i and $i+1$:

$$j^e_{i-1,i} = -k_1 r_{i-1}(p_i + p_{i-1}) = -\nabla\phi_i + L(h_i) \tag{A.4}$$

where L is the generator defined in Eq.(3.11), $\phi_i = \frac{1}{4\lambda}(p_i^2 + k_1 r_i r_{i-1})$, $h_i = -1/(2\lambda) j^e_{i-1,i}$ and ∇ is the discrete derivative $(\nabla\phi)_i = \phi_i - \phi_{i-1}$. Integrating the heat current equation for each site, we have:

$$\begin{aligned}
& N^{-1}\sum_{i=1}^{N} G(i/N)\langle \mathcal{E}_i(tN^2)\rangle - N^{-1}\sum_{i=1}^{N} G(i/N)\langle \mathcal{E}_i(0)\rangle \\
N^{-1} & \sum_{i=2}^{N-1}\int_0^{tN^2} G(i/N)(\langle j^e_{i-1,i}(s)\rangle - \langle j^e_{i,i+1}(s))ds \\
N^{-2} & \sum_{i=2}^{N}\int_0^{tN^2} \frac{G(\frac{i}{N}) - G(\frac{i-1}{N})}{1/N})\langle j^e_{i-1,i}(s)ds \\
\approx\ & N^{-2}\sum_{i=2}^{N}\int_0^{tN^2} G'(i/N)\langle j^e_{i-1,i}(s)\rangle ds \\
\approx\ & N^{-3}\sum_{i=2}^{N}\int_0^{tN^2} G''(i/N)\langle \phi_i(s)\rangle ds \\
& +N^{-2}\sum_{i=2}^{N}\int_0^{tN^2} G'(i/N)\langle (Lh_i)(s)\rangle ds \\
\approx\ & N^{-1}\sum_{i=2}^{N}\int_0^{t} G''(i/N)\langle \phi_x(sN^2)\rangle ds \\
& +N^{-2}\sum_{i=2}^{N} G'(x/N)\left\{\langle h_i(tN^2)\rangle - \langle h_i(0)\rangle\right\} \\
\approx\ & N^{-1}\sum_{i=2}^{N}\int_0^{t} G''(i/N)\langle \phi_i(sN^2)\rangle ds + \mathcal{O}(N^{-1})\,.
\end{aligned} \tag{A.5}$$

In the above derivation, we have used at several steps, the boundary conditions on G and assumed $N \to \infty$ to approximate discrete difference by differentials. From assumption of local thermal equilibrium , with the macroscopic profile given by $u(q,t)$ and $\varepsilon(q,t)$, we have

$$\begin{aligned} \langle \phi_i(tN^2) \rangle &= \frac{1}{4\lambda} \langle p_i^2 + k_1 r_i r_{i-1} \rangle \\ &= \frac{1}{4\lambda} (T(i/N,t) + k_1 u(i/N,t)^2) \\ &= \frac{1}{4\lambda} (\varepsilon(i/N,t) + k_1 u(i/N,t)^2/2) \end{aligned} \tag{A.6}$$

The mean represented above by $\langle . \rangle$ are averages calculated over time scales sufficiently short that the macroscopic profile does not change significantly. We have used the following relations, $\langle r_i(tN^2) \rangle = u(i/N,t)$ and $\langle \mathcal{E}_i(tN^2) \rangle = T(i/N,t) + k_1 u^2(i/N,t)/2$ in the derivation. Plugging Eq.(A.6) back into Eq.(A.5) and taking the limit $N \to \infty$ we obtain the equation of the form given in Eq.(A.3).

The current $j^r_{i-1,i}$ for the deformation can be written as

$$j^r_{i-1,i} = -p_i = -\frac{1}{2\lambda}(\nabla r_i) + L(\frac{1}{2\lambda} p_i). \tag{A.7}$$

By following the same procedure with a test function G satisfying the appropriate boundary conditions, we can show that the the macroscopic deformation satisfies the relation given in Eq.A.3) with $w = u$, $y = u$ and $\sigma = 1/(2\lambda)$.

A.2 Pinned Chain

There is only one quantity that is conserved by the bulk dynamics for this case,i.e, energy. To derive the relation given in Eq.(3.29) for the macroscopic energy profile,

we once again rewrite the expression for the current,

$$j^e_{i-1,i} = -k_1 r_{i-1}(p_i + p_{i-1}) = -\nabla\xi_i + L(h_i) \tag{A.8}$$

where h_i is the same function as defined earlier and

$$\xi_i = \frac{k_1}{4\lambda}(p_i^2 - (k_0 + k_1)q_i^2 - k_1 q_{i-1}q_{i+1} + k_1 q_{i+1}q_i + k_1 q_i q_{i-1}). \tag{A.9}$$

If we carry out a similar expansion as we did for the unpinned case in Eq.(A.5), we will find arrive at an expression of the form Eq.(A.3) with $w = \varepsilon$ and $\sigma(i/N)y(i/N, t) = \langle\xi_i(tN^2)\rangle_t$. As before $\langle.\rangle_t$ is the mean that is calculated on a time scale where the macroscopic profile of energy and deformation does not change appreciably.
Defining $\langle q_i q_j\rangle_T = \theta(i-j)$, and in the bulk where i, j are far from the boundaries, $\theta(z)$ can be regarded as an even function of z. It is the solution to the interaction matrix $\hat{\Phi}$ defined in Eq.(3.1) in the limit $N \to \infty$, i.e, $\hat{\Phi^{-1}}_{i,j} = \theta(i-j)$.

$$(k_0 + 2k_1)\theta(z) - k_1\theta(z-1) - k_1\theta(z+1) = T\delta_{z=0}. \tag{A.10}$$

Performing a Discrete Fourier Transform of Eq. (A.10), we obtain

$$\tilde{\theta}(p) = T/(k_0 + 4k_1 \sin^2(p/2)).$$

Inverting the expression again we get

$$\theta(z) = T\int_0^{2\pi} dp \frac{e^{ipz}}{k_0 + 4k_1\sin^2(p/2)}.$$

We now have :

$$\begin{aligned}
\langle \xi_i(tN^2) \rangle_{T(i/N)} &= \frac{k_1}{4\lambda}(T(i/N,t) - (k_0+k_1)\theta(0) - k_1\theta(2) + 2k_1\theta(1)) \\
&= \frac{k_1}{4\lambda}(T(i/N,t) - k_0(\theta(0)+\theta(1)) \\
&= \frac{k_1}{2\lambda}\frac{1}{k_0+2k_1+\sqrt{k_0(k_0+4k_1)}}T(i/N,t) \\
&= \sigma\varepsilon(i/N,t) \qquad \text{(A.11)}
\end{aligned}$$

where $\varepsilon = T$ and σ is the conductivity which agrees with our result earlier Eq.(3.9).

Appendix B

Boundary Condition

For the unpinned chain, we have that

$$\begin{aligned} \partial_t & \int_0^1 u(q,t)dq = 0 \\ = & \int_0^1 \partial_q^2 u(q,t) \\ \Rightarrow & \ \partial u(0,t) = \partial_q u(1,t) = f(t) \end{aligned} \tag{B.1}$$

where we have used Eq.(3.26) in the second step. To show that $f(t) = 0$ consider the following:

$$Lp_1 = (r_1 - r_0) - (\gamma + 1)p_1, \quad Lr_0 = p_1. \tag{B.2}$$

$$\begin{aligned} \frac{1}{N}\left\{\langle p_1(tN^2)\rangle - \langle p_1(0)\rangle\right\} = & \int_0^t N\left[\langle r_1(sN^2)\rangle - \langle r_0(sN^2)\rangle\right] ds \\ & - (\gamma+1)\, N \int_0^t \langle p_1(sN^2)\rangle ds, \end{aligned}$$

$$\int_0^t \langle p_1(sN^2)\rangle ds = \frac{1}{N^2}\left\{\langle r_0(tN^2)\rangle - \langle r_0(0)\rangle\right\}$$

The second equality shows that $N\int_0^t \langle p_1(sN^2)\rangle ds$ vanishes as N goes to infinity. The left hand side of the first equality is of order $1/N$ and since $\int_0^t N\left[r_1(sN^2) - r_0(sN^2)\right] ds$

converges to $\int_0^t (\partial_q u)(0,s)ds = \int_0^t f(s)ds$, we have $f(s) = 0$ for any s.quality shows that $N\int_0^t \langle p_1(sN^2)\rangle ds$ vanishes as N goes to infinity. The left hand side of the first equality is of order $1/N$ and since $\int_0^t \; N\left[r_1(sN^2) - r_0(sN^2)\right] \, ds$ converges to $\int_0^t (\partial_q u)(0,s)ds = \int_0^t f(s)ds$, we have $f(s) = 0$ for any s.

Bibliography

[1] P.G. Bergmann and J.L. Lebowitz, *New Approach to Nonequilibrium Processes*, Phys. Rev. **99**, 578 (1955); J.L. Lebowitz and P.G. Bergmann, *Irreversible Gibbsian Ensembles*, Ann. Phys. **1**,1 (1957)

[2] Z. Rieder, J.L. Lebowitz and E. Lieb, *Properties of a Harmonic Crystal in a Stationary Nonequilibrium State*, J. Math. Phys., **8**, 1073 (1967).

[3] A. Casher and J. L. Lebowitz, *Heat Flow in Regular and Disordered Harmonic Chains*, J. Math. Phys. **12**, 1701 (1971).

[4] A. Dhar and D. Roy, *Heat Transport in Harmonic Lattices*, J. Stat. Phys. **125**, 801 (2006).

[5] C. Kipnis, C. Marchioro and E. Presutti, *Heat flow in an exactly solvable model*, J. Stat. Phys. **27**, 85 (1982)

[6] Brian Ryals and Lai-Sang Young, *Nonequilibrium Steady States of Some Simple 1-D Mechanical Chains*, J. Stat. Phys., **146**, 1089 (2012)

[7] K. Aoki and D. Kusnezov, *Fermi-Pasta-Ulam β Model: Boundary jumps, Fouriers law, and scaling*, Phys. Rev. Lett. **86**, 4029 (2001).

[8] S. Lepri, R. Livi and A. Politi, *Studies of thermal conductivity in Fermi-Pasta-Ulam like lattices*, Chaos **15**, 015118 (2005).

[9] T. Hatano, *Heat conduction in the diatomic Toda lattice revisited*, Phys. Rev. E **59**, R1

[10] J. Lukkarinen and H. Spohn, *Anomalous Energy Transport in the FPU β chain*, Comm. Pure App. Math.**61**, 1753 (2008).

[11] B. Hu and L. Yang, *Heat Conduction in the Frenkel-Kontorova model*, Chaos **15**, 015119(2005).

[12] B. Hu, B. Li and H. Zhao, *Heat conduction in one-dimensional nonintegrable systems*, Phys. Rev. E **61**, 3828 (2000)

[13] R. Lefevere and A. Schenkel, *Normal heat conductivity in a strongly pinned chain of anharmonic oscillators*, J. Stat. Mech. **L02001** (2006)

[14] K. Aoki, J. Lukkarinen and H. Spohn, *Energy Transport in Weakly Anharmonic Chains*, J. Stat. Phys. **124**, 1105 (2006)

[15] A. Lippi and R. Livi, *Heat Conduction in Two-Dimensional Nonlinear Lattices*, J. Stat. Phys. **100**, 1147 (2000)

[16] H. Shiba and N. Ito, *Anomalous Heat Conduction in Three-Dimensional Nonlinear Lattices*, J. Phys. Soc. Jpn. **77**, 054006 (2008)

[17] E. Pop, D. Mann, Q. Wang, K. Goodson, and H. Dai, *Thermal Conductance of an Individual Single-Wall Carbon Nanotube above Room Temperature*, Nano. Lett. **6** , 96 (2006)

[18] Z.L. Wang et al, *Length-dependent thermal conductivity of an individual single-wall carbon nanotube*, App. Phys. Lett. **91**, 123119 (2007)

[19] C. W. Chang, D. Okawa, H. Garcia, A. Majumdar, and A. Zettl, *Breakdown of Fouriers Law in Nanotube Thermal Conductors*, Phys. Rev. Lett. **101**, 075903 (2008)

[20] H. Nakazawa, *On the Lattice Thermal Conduction*, Suppl. Prog. of Theo. Phys., 45, 231 (1970).

[21] H. Risken, *The Fokker Planck equation* (Springer, Berlin, 1989).

[22] A. Dhar, *Heat Conduction in the Disordered Harmonic Chain Revisited*, Phys. Rev. Lett., **86**, 5882 (2001)

[23] R. Rubin and W. Greer,*Abnormal Lattice Thermal Conductivity of a OneDimensional, Harmonic, Isotropically Disordered Crystal* , J. Math. Phys., **12**, 1686 (1971)

[24] H. Matsuda and K. Ishii, *Localization of Normal Modes and Energy Transport in the Disordered Harmonic Chain*, Suppl. Prog. Theor. Phys., **45**, 56 (1970)

[25] G. Basile, C. Bernardin and S. Olla, *Thermal Conductivity of a Momentum Conservative Model*, Comm. in Math. Phys., **287**, 67 (2009)

[26] C. Bernardin and S. Olla, *Fourier's Law for Microscopic Model of Heat Conduction*, J. Stat. Phys, **121**, 271 (2005)

[27] M. Bolsterli, M. Rich, and W. M. Visscher, *Simulation of nonharmonic interactions in a crystal by self-consistent reservoirs* , Phys. Rev. A 4:10861088 (1970)

[28] L. Delfini, S. Lepri, R. Livi, and A. Politi, *Nonequilibrium Invariant Measure under Heat Flow*, Phys. Rev. Lett. **101**, 120604 (2008).

[29] F. Bonetto, J. L. Lebowitz, and J. Lukkarinen, *Fourier's law for a harmonic crystal with self-consistent reservoirs*, J. Stat. Phys. **116**, 783 (2004).

[30] H. Mori, *Statistical-Mechanical Theory of Transport in Fluids*, Phys. Rev. 112, 1829 (1958)

[31] R. Kubo, M. Yokoto and S. Nakajima, *Statistical-Mechanical Theory of Irreversible Processes. II. Response to Thermal Disturbance*, J. Phys. Soc. Jpn **12**, 1203 (1957)

[32] C. Bernardin, *Thermal Conductivity for a Noisy Disordered Harmonic Chain* , J. Stat. Phys. **133**, 417 (2008)

[33] S. Sethuraman *Central Limit Theorem for additive functionals of the simple exclusion process*, The Annals of Probability **28**, 277-302 (2000).

[34] A. Dhar and J.L. Lebowitz, *Effect of phonon-phonon interactions on localization*, Phys. Rev. Lett. **100**, 134301 (2008).

[35] O. Ajanki and F. Huveneers, *Rigorous scaling law for the heat current in disordered harmonic chain*, Commun. Math. Phys. **301**, 841 (2011)

[36] T. Verheggen, *Transmission coefficient and heat conduction of a harmonic chain with random masses: asymptotic estimates on products of random matrices*, Commun. Math. Phys., **68**, 69(1979).

[37] T. Mai, A. Dhar, O. Narayan, *Equilibration and Universal Heat Conduction in Fermi-Pasta-Ulam Chains* , Phys. Rev. Lett., **98**, 184301 (2007)

[38] C. Bernardin, *Hydrodynamics for a system of harmonic oscillators perturbed by a conservative noise*, Stoch. Process. Appl. **117**, 487–513, (2007)

[39] A. Dembo and O. Zeitouni,*Large deviations techniques and applications*, 2nd ed., Springer, Application of Mathematics vol. **38**, (1998)

[40] L. Bertini, A. De Sole, D. Gabrielli, G. Jona-Lasinio, C. Landim, *Macroscopic fluctuation theory for stationary non equilibrium state,* J. Stat. Phys. **107**, 635–675, (2002)

[41] L. Bertini, D. Gabrielli, J.L. Lebowitz, *Large deviations for a stochastic model of heat flow*, J. Stat. Phys. **121**, 843–885, (2005)

[42] A.L. Wang et al., *Length-dependent thermal conductivity of an individual single-wall carbon nanotube*, Appl. Phys. Lett. 91, 123119 (2007)

[43] C.W. Chang et al., *Breakdown of Fouriers Law in Nanotube Thermal Conductors*, Phys. Rev. Lett. 101, 075903 (2008)

[44] N. Li and B. Li, *Parameter dependent conductivity of one dimensional ϕ^4 lattice*, Phys. Rev. E, 76, 011108 (2007)

[45] G. Casati, J. Ford, F. Vivaldi and W.M. Visscher, *One-Dimensional Classical Many-Body System Having a Normal Thermal Conductivity* Phys. Rev. Lett. 52 (1984) 1861.

[46] D.J.R. Mimnagh and L.E. Ballentine, *Thermal conductivity in a chain of alternately free and bound particles* , Phys. Rev. E 56 (1997) 5332.

[47] M.J. Gillan and R.W. Holloway,*Transport in the Frenkel-Kontorova model. III. Thermal conductivity*, J. Phys. C **18**, 5705 (1985)

[48] G.P. Tsironis, A.R. Bishop, A.V. Savin and A.V. Zolotaryuk,*Dependence of thermal conductivity on discrete breathers in lattices* , Phys. Rev. E 60 (1999) 6610

[49] C. Bernardin *Private Communication*

[50] C. Bernardin, *Thermal Conductivity for a Noisy Disordered Harmonic Chain* , J. Stat. Phys.**133**, 417 (2008)

[51] C. Bernardin, V. Kannan, J.L. Lebowitz and J. Lukkarinen, *Harmonic Systems with Bulk Noises*, J. Stat. Phys. **146**, 800 (2012)